



POLITECNICO DI TORINO
Department of Electronic Engineering

Laser induced graphene as electrode for wearable electronic devices

Author:

Chiara Ballin
S241472

Supervisor:

Dr. Andrea Lamberti

Dicember 2018

ABSTRACT

Laser-induced Graphene(LIG) is a porous material obtained by graphenization of polymeric substrate. The fabrication approach consists of exploiting the use of pulsed-laser writing, causing the absorption of long-wavelength radiation, which produces photo-thermal effects. The purpose is to obtain Graphene from a wide range of carbon precursors under ambient atmosphere conditions. LIG opens up a lot of new ways in electronics, especially for flexible, biodegradable and edible electronics. Thanks to this technique conductive patterns can be obtained on planar and flexible substrates and used as electrodes for strain sensors and supercapacitors (SCs). The substrate used, in my thesis, is polydimethylsiloxane(PDMS) because of its wide use due to its rheological properties, low cost and biocompatibility. The resulted LIG patterns on PDMS are characterized in order to study conductivity. To improve it, a variation of laser parameters (power, frequency, velocity and others) is performed and different substrates mixed with PDMS are tested. The best mix results using triethylene glycol (TEG) and a study varying its percentage inside PDMS matrix is carried out. The optimum laser parameters onto pure PDMS and PDMS-TEG mixture are used to write strain sensors and supercapacitors. The samples were also analyzed by Scanning Electron Microscopy and Raman spectroscopy. Sheet Resistance are evaluated in 'flat and bending conditions'. The performances of SCs are obtained with electrical/electrochemical measurements such as cyclic voltammetry, electrochemical impedance spectroscopy and constant current charge/discharge. A final comparison between PDMS and PDMS-TEG in strain gauges and supercapacitors is carried out. An excellent result is that PDMS-TEG(40% in-weight) has a specific capacitance 200 times higher than pure PDMS-based devices.

DEDICATION AND ACKNOWLEDGEMENTS

First of all i would like to thank Dr. Andrea Lamberti for giving me the possibility to do this research about a new interesting argument, never treated during the university courses.

A special thanks is also for Pietro Zaccagnini that follow me and give me his support during this months.

I'm very grateful to Alessandro Pedico and Giorgio Auxilia for their help and willingness. For the experimental part i would like to thank a lot of DISAT members, like Stefano Stassi, Stefano Bianco, Marco Fontana.

My gratitude is for Microla team of Chivasso that have assisted me during the laser writing part and they have always been so kind and helpful.

Finally an huge thank is for all my family that have supported and encouraged me during all this long five years of study.

AUTHOR'S DECLARATION

I declare that the work in this dissertation was carried out in accordance with the requirements of the University's Regulations and Code of Practice for Research Degree Programmes and that it has not been submitted for any other academic award. Except where indicated by specific reference in the text, the work is the candidate's own work. Work done in collaboration with, or with the assistance of, others, is indicated as such. Any views expressed in the dissertation are those of the author.

SIGNED: DATE:

TABLE OF CONTENTS

	Page
List of Tables	ix
List of Figures	xi
1 Introduction	1
1.1 Wearable electronics	1
1.2 Graphene	5
1.3 LIG: Laser induced graphene	7
1.4 PDMS: polydimethylsiloxane	9
1.4.1 Brief description of mechanical and chemical PDMS properties . .	10
1.4.2 Application of PDMS	11
2 Background theory	13
2.1 Strain sensors	13
2.1.1 Types and materials of strain gauge	15
2.1.2 Application of strain gauges	16
2.2 What is a supercapacitor?	17
2.2.1 Supercapacitor structure	18
2.2.2 Materials of SCs	19
2.2.3 Supercapacitor performance evaluation	21
3 Laser writing set up & material characterization	29
3.1 Laser description and operation	30
3.1.1 Parameters variation	31
3.1.2 Geometries	31
3.2 Characterization of substrates	32
3.2.1 LIG lines on PDMS substrate	33

TABLE OF CONTENTS

3.2.2	LIG lines on PDMS-TEG substrate	35
3.2.3	LIG lines on different substrates	37
3.3	Raman Spectroscopy and Scanning electron microscope	39
3.3.1	Raman Spectroscopy	39
3.3.2	Scanning electron microscope	42
3.3.3	Mechanical tests	45
4	Devices fabrication and characterization	47
4.1	Strain sensors	47
4.1.1	LIG strain sensors on PDMS substrate	48
4.1.2	LIG strain sensors on TEG substrates	49
4.1.3	LIG Strain sensors on different substrates	51
4.2	Supercapacitors	53
4.2.1	LIG supercapacitor on PDMS substrate	53
4.2.2	LIG supercapacitor on TEG substrates	56
4.2.3	Comparison between LIG supercapacitor on different percentage of TEG into PDMS substrate	62
4.2.4	Comparison between LIG supercapacitor on PDMS and PDMS- TEG substrates	64
5	Conclusion	67
5.1	Main results	67
5.2	Possible improvements	77
	Bibliography	79

LIST OF TABLES

TABLE	Page
3.1 Working parameters of laser writing	33
3.2 Main applications of TEG [7]	35
3.3 Working parameters of laser writing	40
4.1 Working parameters of laser writing of PDMS-TEG strain sensors	49
4.2 Summary of the C_S results obtained from the Cv of different percentage of TEG into PDMS	63

LIST OF FIGURES

FIGURE	Page
1.1 Schematic representation of the different prospects of wearable flexible devices [5]	2
1.2 Common examples of wearable sensor technologies [18]	4
1.3 Carbon atoms bonded in graphene structure [8]	5
1.4 Allotropes of carbon: 2-D graphene, 0-D fullerene, 1-D carbon nanotube, 3-D graphite [8]	6
1.5 Scheme of LIG fabrication process onto polyimide (PI) [1]	7
1.6 Microsupercapacitor fabricated on coconut [22]	8
1.7 Defocusing technique for obtain an increase spot size [22]	9
1.8 Chemical structure of PDMS and tridimensional representation [14]	10
1.9 Example of supercapacitor made onto PDMS substrate	11
1.10 The developed microfluidic analyzer of Ref. [2] background system is able to analyze, measure biological liquids and calculate the number of morphological well-separated different elements with optical and electrical way.	12
2.1 Basic scheme of a common type of strain gauges [21]	14
2.2 One-step fabrication of artificial throat made exploiting LIG [12]	16
2.3 Example of human finger motion detection with stretchable carbon traces [16]	17
2.4 Schematic diagram of (A) electrostatic capacitor, (B) EDL capacitor, (C) PCs, (D) hybrid-capacitor [6]	19
2.5 Schematics of conventional SC structure on the left side and of the interdigitated structure on the right side [11]	20
2.6 Scheme pf key performance test methods and metrics for evaluate SCs	22
2.7 Simplified equivalent circuit of SCs	23
2.8 Typical CV, in black the potential applied, in blue the typical current plot obtained for a supercapacitor vs time [23].	24

2.9	Typical CCCD, in blue the current imposed, in black the typical potential vs time plot obtained for a supercapacitor [23].	25
2.10	Example of Nyquist plot for the circuit represented in figure.	27
3.1	Laser CO_2 present in Microla Optoelectronics laboratory in Chivasso	30
3.2	Geometries designed with Rhino 6 CAD software used in laser writing, each square of the grid is 1X1mm	32
3.3	Plot of Sheet Resistance vs Frequency varying laser parameters according to table 3.1	34
3.4	Comparison between Sheet Resistance of the PDMS lines written in inert ambient (Right fig.) or no (left fig.)	34
3.5	Trend of R_S increasing the percentage of TEG into PDMS	36
3.6	Comparison between lines written onto a substrate, made of a mixture of PDMS and TEG, and another substrate, made of a mixture of PDMS and KEVLAR.	38
3.7	Pictures of the substrates made of percentage of Kevlar specify in the text	39
3.8	Raman of LIG on PDMS	41
3.9	Raman of characterization of LIG onto PDMS-TEG in the 4 different % presented in section 3.2.2	42
3.10	Comparison between Raman of LIG on PDMS and PDMS-TEG 40%	43
3.11	Fesem of PDMS-TEG mixture at a scale of 200 μm and 20 μm	44
3.12	Instron model 2712-003, machine use to perform mechanical tests	45
3.13	Young's module plot versus the deformation $\Delta l = l - l_0$	46
4.1	Strains made on pure PDMS substrates written at the same frequency of 15 kHz and 2 repetitions	48
4.2	Value of R_S of PDMS-TEG strain for different substrates and parameters of laser writing	50
4.3	variation OF $\Delta R/R_0\%$ testing the bending of the PDMS-TEG device with different bending radius	50
4.4	According to the bending of the device the $\Delta R/R_0\%$ there is a strong variation in $\Delta R/R_0\%$ in line4 of Ice substrate	51
4.5	Electrochemical measurements of PDMS supercapacitor	54
4.6	Cyclic voltammetry at 10 mV/s of a supercapacitor made onto polymide [1]	55
4.7	Electrochemical measurements of PDMS-TEG 10% supercapacitor	56
4.8	Electrochemical measurements of PDMS-TEG 20% supercapacitor	58

4.9	Electrochemical measurements of PDMS-TEG 30% supercapacitor	59
4.10	Electrochemical measurements of PDMS-TEG 40% supercapacitor	60
4.11	Electrochemical measurements, CV (at 50 mV/s) and CCCD ($I = 1 \mu A$), of PDMS-TEG Sc, varying the % in weight of TEG	62
4.12	Comparison between cyclic voltammetry at 10 mV/s of LIG SC on PDMS (red) and PDMS-TEG 40% (black)	64
4.13	Constant Current charge/discharge of PDMS and PDMS-TEG supercapacitors	65
5.1	Supercapacitor made onto pure PDMS substrate with laser induced graphene	68
5.2	Sheet Resistance variation increasing the percentage of TEG into PDMS . . .	69
5.3	Comparison between the CV and CCCD of LIG SC for different percentage of TEG into PDMS	70
5.4	Comparison of Raman spectroscopy	71
5.5	Scanning electron microscopy (SEM) of PDMS-TEG 40% line. There is a zoom onto the deep crevice located at the beam center.	72
5.6	Comparison between CV and CCCD of LIG supercapacitors made onto 'pure' PDMS and PDMS-TEG 40%	73
5.7	Ragone's plots of PDMS, PDMS-TEG 10%, PDMS-TEG 20%, PDMS-TEG 30%, PDMS-TEG 40% and Ref. [1] Supercapacitors	74
5.8	Ragone's plots of PDMS-TEG 10%, PDMS-TEG 20%, PDMS-TEG 30%, PDMS-TEG 40% and Ref. [1] Supercapacitors	75

INTRODUCTION

In this first chapter it is introduced, firstly, the concept of wearable electronics, explaining in the details the problems related to power the devices inserted in this category. Due to the huge popularization of wearable flexible devices the development of compact energy storage systems, as supercapacitors, has accelerated.

A lot of graphitic carbon nanomaterials, as graphene (1.2) or single-walled carbon nanotubes are used as electrodes.

Thirdly a new material, called laser induced graphene (LIG), that opens a lot of new ways in electronics, is described. This is due to the fact that it is possible to obtain patterned graphene on the surface of a various range of material exploiting laser scribing under ambient atmosphere conditions.

Finally PDMS, used herein as substrate to be converted into LIG, is described in detailed in section 1.4 in order to highlight its different positive features and because it is a common and cheap polymer extensively used in a wide range of applications.

1.1 Wearable electronics

Starting the advent of home security monitoring systems more than a decade ago, as shown in Ref. [5] the era of wearable electronics and internet of things (IoT) began. Nowadays there are complicated systems that monitor glucose levels, blood pressure, heart rate and a lot of other body parameters. It is possible to say that only imagination constrains the potential for wearable electronics. Thanks to smart textiles there is a

continuous expansion of possibilities, there is a direct integration of sensors into woven fabrics. The application of wearable electronics are enormous, including baby monitoring, healthcare, automotive and also military one in particular for batteries, antennas, vital sign monitoring sensors.

In fig. 1.1 there is a basic scheme that represents the wearable electronics view from different prospects. There are divided into two parts: on the right side some devices are listed: chemiresistors, electrodes, organic thin film transistors sensors, smart textiles, organic electronic ion pump. Instead on the left side features that the materials have to possess are present, for example, flexibility, solubility, biocompatibility and stability are some. According to market actual requirements the development is always in progress,

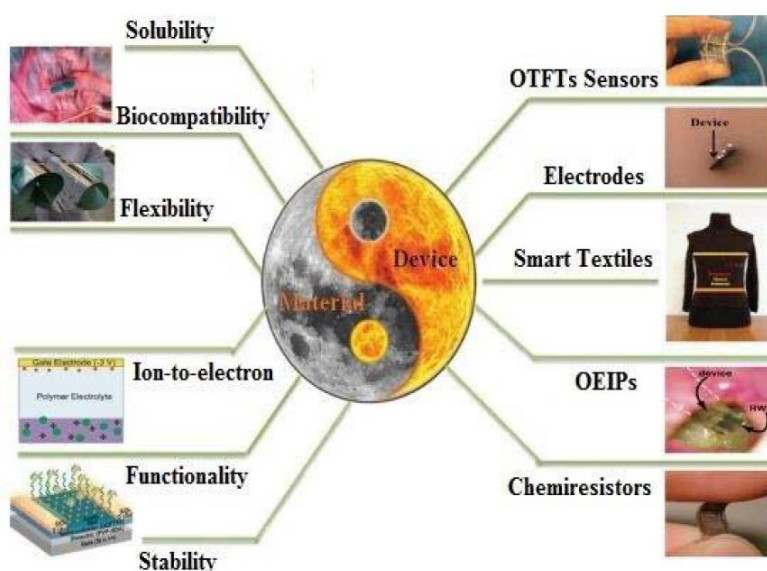


Figure 1.1: Schematic representation of the different prospects of wearable flexible devices [5]

regarding the evolution in manufacturing, device packaging, cost management, materials and a lot of other issues. Sensors can be divided in two macro-categories: non-flexible and flexible ones [3].

The non-flexibles ones have been developed earlier compared to the second category, in particular the sensors with silicon substrates are the most common. The drawbacks of them are a lot, one of the majority is stiffness, in particular the application of it during the monitor of physiological parameters of people results difficult because of the high stress that could damage the non-flexible sensor.

Flexible sensors have become nowadays a better options for wearable electronics thanks

to its low fabrication cost, good thermal and mechanical properties, light weight, etc. The most common materials nowadays used to develop these sensors are polydimethylsiloxane (PDMS), polyethylene naphthalate (PEN), Polyimide (PI), Parylene and others.

Instead for electrode part of these sensors, carbon-based materials are often used. This category of materials include carbon nanotubes (CNTs), carbon fibers, graphene (section 1.2), LIG (section 1.3). The most famous type of flexible sensors are the electrochemical ones, in particular they represent an excellent choice for biochemical sensing, for example for monitoring cholesterol, glucose, pH, etc.

Another type of sensors, as shown in Ref. [3], is the pressure one. This kind of sensors are for tactile sensing and artificial intelligence, they had been often manufactured as electronic bandages. Indeed to monitor physiological parameters the sensors widely employed used are the piezoresistive ones. Their working principle consists in varying the resistivity of the material when a stress is applied instead the strain gauges exploit the variation in resistance due to a change in the geometry of the sensor.

Due to this also a lot of tactile sensors exploit metal piezoresistors either with simple geometry or as strain gauges, in order to combine two positive features: resistivity and geometrical variation [17]. Strain sensors, that are treated in this master thesis deeply described in section 2.1, explaining the meaning of gauge factor (GF), tensile and compressive strain.

Another big category is the one of magnetic field sensors which exploit the use of inorganic functional nano-membranes with polymeric foils.

Due to this huge development and popularization of wearable sensors the strong necessity of wearable energy storage devices comes out. In particular the study in flexible/stretchable energy storage devices has accelerated because they possess remarkable characteristics of high security, ease integration, capacity of delivering energy at a very fast rate and a lot of other features, all well described in chapter 2.

Into these crowd of storage devices, the supercapacitors stand out with a certain preponderance compared to others, as for example rechargeable batteries. This is due to the fantastic characteristics of SCs that lead to numerous advantages. Nowadays various flexible supercapacitors (FSCs) and flexible electrodes (FEs) have a key role because of the interest in portable and wearable electronic equipment, in fact their use has increased sharply.

The most evident benefits of SCs that must be underlined are the low cost, the ease fabrication, the longer life duration compared with the others, as for examples the lithium-ion batteries but also it is possible to highlight their bigger power, a very important param-

ters in the sensors field.

A huge development in SCs is conducted by Army Forces in order to guarantee autonomy of wearable, in particular this devices are direct incorporated into military uniforms. For example in fig.1.2 an image representing a soldier full of wearable devices is shown. He wears glasses equipped with sensors able to detect the presence of chemical substances, GPS, data reader and others. Then he wears an uniform, made with smart textiles in order to monitor physiological parameters, and also smart 'keychains' to detect air quality, temperature, humidity, radiation, luminosity etc. It is present also a futuristic smart tattoo with medical and enviromental sensing that can control blood, pressure, temperature, give vibrating alert. Finally a smart watch, common nowadays, that can do a multitude of different things, starting from catch biometric data until reach messages and calls.



Figure 1.2: Common examples of wearable sensor technologies [18]

These are only few of the future trends that are in develop not only for military purposes but also for civilian ones. Due to this, textiles-based and biocompatible supercapacitors must be incorporated and used with some necessary features like security, reliability and comfortability.

To achieve these tasks a lot of materials have been developed and caught the market thanks to their extraordinary properties. One of these materials is graphene, described in section 1.2, which has become predominant in the wearable electronic military world and, more in general, in wearable technology.

1.2 Graphene

Graphene was synthesized by Andre Geim and Konstantin Novoselov in 2004 at the University of Manchester. It is a two dimensional single layer of sp^2 bonded carbon

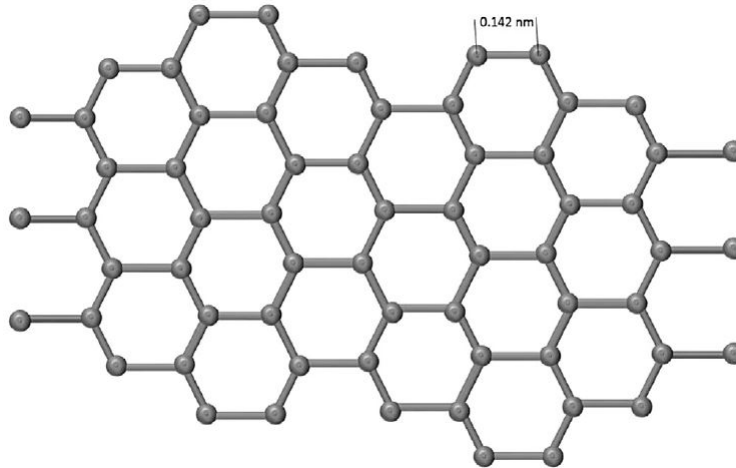


Figure 1.3: Carbon atoms bonded in graphene structure [8]

atoms arranged in a hexagonal lattice [8]. It is a sort of building block for all graphitic materials. The atoms of carbon are bonded at a length of 0.142 nm, clearly indicated in fig.1.3.

As easy summarized in fig.1.4, it can be wrapped up into zero-dimensional (0-D) fullerenes, rolled into one-dimensional (1-D) nanotubes, stacked into three-dimensional (3-D) graphite.

Graphene exhibits extraordinary mechanical and chemical properties related to thermal conductivity ($5000 \text{ W m}^{-1} \text{ K}^{-1}$, excellent value), surface area ($2630 \text{ m}^2 \text{ g}^{-1}$), Young's modulus (1 TPa, very high), excellent gas impermeability despite only being single atom thick, light transmittance (around 98%, very high).

Pure graphene sheets are mostly unreactive, the surface needs to be functionalized in order to be chemical reactive with other materials. There is also a dependence of thickness, in fact a single layer graphene is almost ten times more reactive than the bi- or multi-layer one.

A modification can be used to generate a band gap useful for application in the semiconductor industry for example in developing devices such as transistors. One of the major challenges regarding graphene, according to paper [8] was the difficulty in finding a procedure to produce it in large scale.

The current techniques to obtain graphene are listed in Ref. [8]. The described methods are epitaxial growth of it on SiC, Silicon carbide, on TiC, Titanium carbide, on TaC,

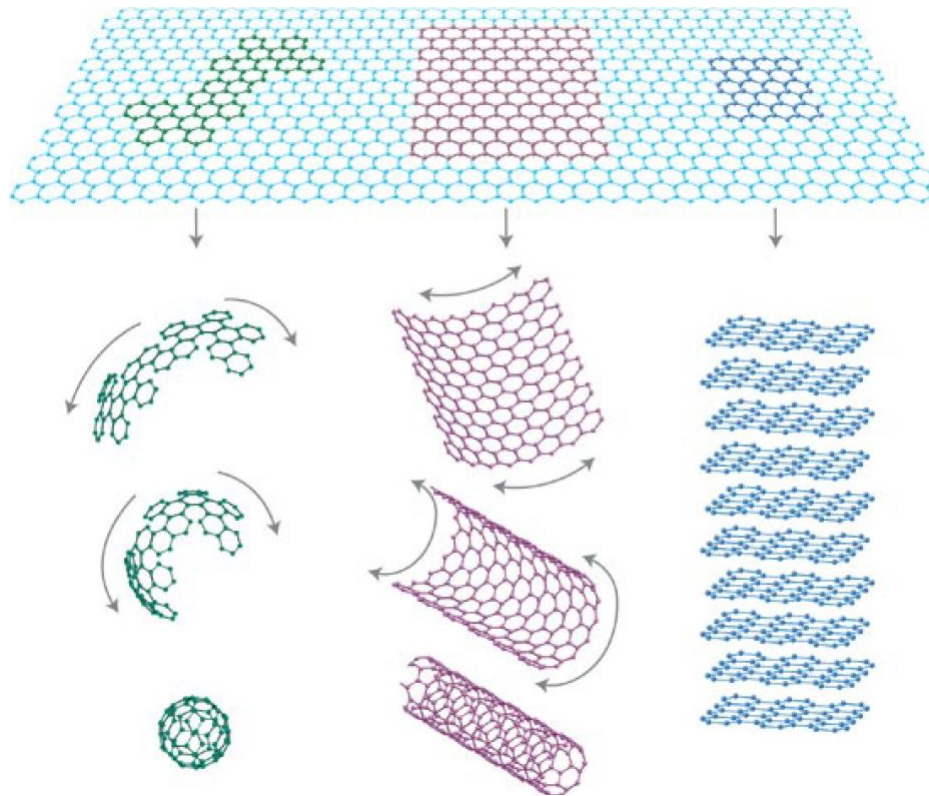


Figure 1.4: Allotropes of carbon: 2-D graphene, 0-D fullerene, 1-D carbon nanotube, 3-D graphite [8]

Tantalum carbide and other different metals. Other techniques include graphene formed from un-zipping of carbon nanotubes, chemical vapour deposition (CVD), organic synthesis, synthesis of it from graphite oxide through oxidation of graphite.

Another low cost, non-toxic, sustainable method is the production from biomass but the optimized methodology to obtain high quality graphene is still running.

To achieve this task of large scale production multiple pulsed laser scribing could be used to obtain patterned graphene onto the surface of different substrates under ambient conditions, the obtained material is called laser induced graphene and it is explained in section 1.3.

1.3 LIG: Laser induced graphene

In 2014 at Rice university James Tour and his colleagues published a paper in which they firstly reported the formation of a porous few-layer graphene by direct-laser writing of Polyimide substrate, calling this material "laser-induced graphene"(LIG) [22]. It is a foam of graphene sheets with one edge attached to the underlying surface. Changing the laser power also the chemical composition and thermal stability of the resulting LIG change, that it is an important feature that it is analyzed in detailed in section 3.1.

A simple method to obtain, under ambient conditions, patterned graphene using multiple

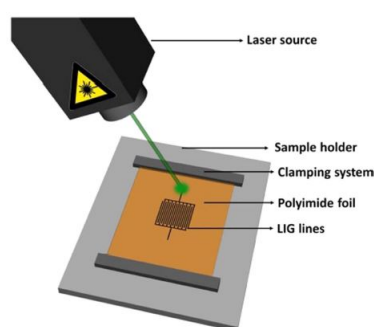


Figure 1.5: Scheme of LIG fabrication process onto polyimide (PI) [1]

lasing is introduced in the paper [22]. With this technique it is possible to convert different and wide range of substrates like paper, cloths, wood, food and also polymers. J.Tour et al. [22] affirmed that by using this method is possible to convert any carbon precursor, that can become amorphous carbon, into graphene. This opens a lot of new ways in electronics, in particularly for flexible, biodegradable and edible electronics. As a proof of concept a micro-supercapacitor was fabricated on a coconut by means of multiple lasing (Fig. 1.6)[22],

In this Ref. [22] a lot of polymers were converted into LIG with success and they are listed below:

- Poly(mphenylenediamine) isophthalamide
- Polyamide Imide (PAI)
- Polyether sulfone (PES) poly(paraphenyleneterephthalamide)Kevlar
- Polybenzimidazole(PBI)
- Polyether ether ketone(PEEK)
- Polyphenylene sulfide (PPS)

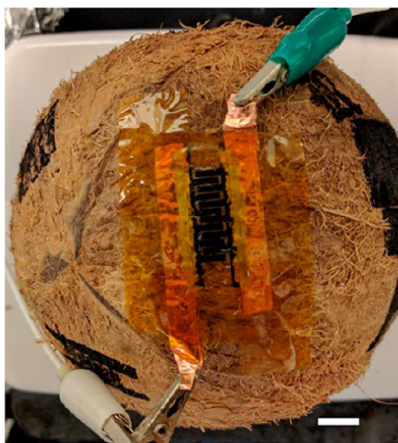


Figure 1.6: Microsupercapacitor fabricated on coconut [22]

- Chlorinated poly(vinyl chloride) (CPVC)
- Thermoset Materials polystyrene (crosslinked)
- Natural Polymer Materials: lignin varies various cellulose (phosphate treated)
- Nonpolymeric Materials activated carbon

In order to improve electrical properties of LIG James Tour and his team use multiple lasing, in particular two methods were used to obtain multiple lases of a substrate. The first, the obvious one, consists in multiple passes of the rastered laser beam.

This method is also used during the experimental part of this master thesis work.

The second method consists in increasing the spot size but keeping the density of the dots consistent. The implementation of this methods was based on a defocusing technique that vary the distance between the laser source and the target substrate, exploits the fact that the focused laser beam is conical.

The concept is clarified by fig. 1.7 [22]. Increasing the defocus settings, the structure of LIG become composed by larger flakes, implying also an improvement in sheet resistance. A great advantage of multiple lasing is the reduction in ablation and thermal damage. Another way, used in paper [22] to improve LIG properties is the addition of fire-retardant materials.

The fact that is important to underline is that multiple lasing gives the possibilities almost any carbon precursor, which doesn't ablate if exposed to CO_2 , to be converted into LIG.

In paper [22] it is demonstrated that any materials that is possible to convert into amorphous carbon can be converted in LIG using multiple lasing.

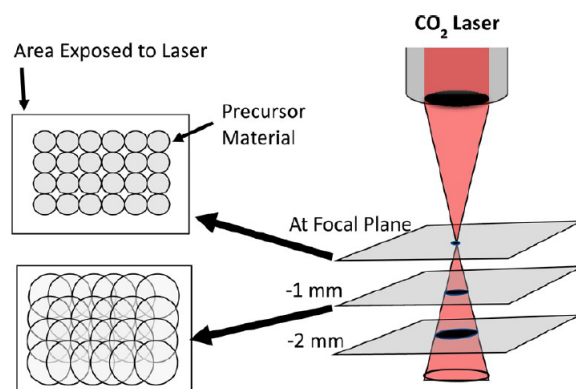


Figure 1.7: Defocusing technique for obtain an increase spot size [22]

However in the crowd of polymer already tested there are not elastomers but only the ones listed before. The elastomers would allow to enhance the performances of wearable, flexible and stretchable devices. A material is called elastomer when is able to be subjected to relevant deformations under stress quite small but if the stress is removed they can come back quickly to the initial shape and dimensions. The one chose in this master thesis thanks to its properties is PDMS, polydimethylsiloxane (Section 1.4).

1.4 PDMS: polydimethylsiloxane

In general polysiloxanes are a class of polymer where the repeat unit contains alternating Oxygen and Silicon atoms with organic groups bound to each Silicon atom. PDMS is inside the category of polymeric organosilicon compounds and it is the widest used, in particular for its rheological properties.

The chemical formula of this material is



and its empirical formula is $(C_2H_6OSi)_n$

In fig. 1.8 is shown the chemical structure and a tridimensional representation.

According on the size of 'n', the monomeric chain, the non cross-linked PDMS may be semi-solid if 'n' is high or could be almost liquid if 'n' is low. PDMS used in this research is PDMS Sylgar©184 (Dow Corning Corporation), this is provided in two part kit: oligomer (siloxane base) and cross-linker (curing agent) components. When these parts are mixed

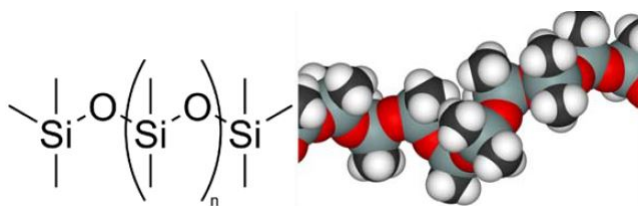


Figure 1.8: Chemical structure of PDMS and tridimensional representation [14]

and subjected to curing at temperature, the crosslinking process takes place and the reticulated elastomer is obtained.

The oligomer PDMS base contains a certain number of vinyl terminated instead the curing agent has 3 silicon hybrid bond for each molecule and an amount of platinum that behaves as catalyst. When the double bond between the vinyl group and the oligomer breaks there is the formation of the following bond $-Si-CH_2-CH_2-Si-$ exploiting one end of the curing agent (-Si-H).

1.4.1 Brief description of mechanical and chemical PDMS properties

This material is viscoelastic so at low temperature it acts like and elastic solid otherwise as a viscous liquid. After cross-linking it has an hydrophobic surface so it's difficult for polar solvent to wet the surface. In order to obtain an hydrophilic surface it is possible to exploit the use of plasma oxidation (air or argon plasma) but in air the oxidized surface is stable only 30 minutes, more or less [19]. However whether on the surface plasma oxidized is or not performed, it does not allow some compounds like water, glycerol, methanol or ethanol.

It swells when there is the presence of diisopropylamine and chloroform, but also it doesn't like propanol, acetone and pyridine.

In fig. 1.9 it is shown a supercapacitor made onto PDMS substrate, the flexibility is clear.

Mechanical strength of polysiloxanes is not good so they must be cross-linked in order to form elastomers or often they are reinforced with fillers, in particular Silica [14]. It is possible to vary the mechanical properties varying the mixing ratio or the oligomer molecular weight in order to obtain different degrees of strength and Young's module (the nominal one for a mixing ratio 10:1 is 0.75 MPa).

However the 0.75 MPa value can be increased with a ratio of 3:1 or reduce with a mixing ratio of 30:1 It results transparent at optical frequencies that range between 240 nm and 1100 nm, this is a good property if it is necessary to observe the content inside

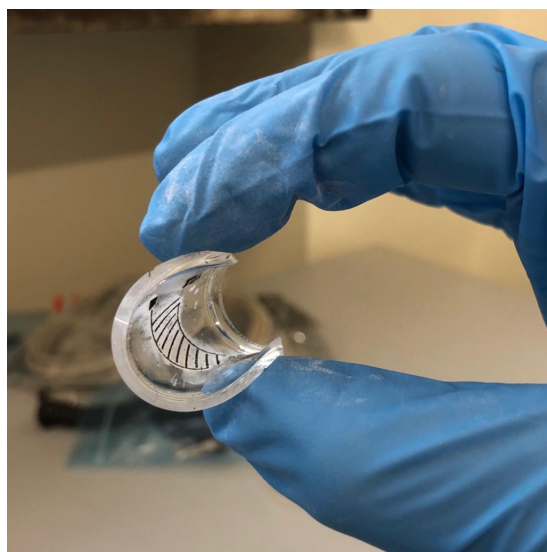


Figure 1.9: Example of supercapacitor made onto PDMS substrate

micro-channels. Its autofluorescence is low. By means of a simple plasma treatment it bonds firmly with another PDMS layers and glass. It offers a lot of advantages in technological possibilities because allow a multilayers production of PDMS.

Polysiloxanes, in general, have good properties related to thermo-oxidative stability, UV and ozone resistance, low surface energy, low glass transition temperature ($T_g = -123^\circ C$), biological inertness.

Compared with others materials, e.g. Silicon, PDMS is inexpensive. It could be integrated into microfluidic valves because it is deformable, another good property. It remains almost liquid at room temperature for many hours also after the mix with the cross-linking agent so it is easy to mould.

Because of its gas permeability it enables cell culture.

1.4.2 Application of PDMS

The use of PDMS in nowadays life is very common, it is present in a lot of cathegory. It is used a lot in medicine, for example in contact lenses, but also in cosmetics for skin and hair products. The strong presence of this material is also in food, in particular fast food where is added to cooking oils. The indirect familiar everyday life with this material is in silicon based lubricants, hair conditioners, Silly Putty, Kinetic Sand (a toy).

PDMS is present in soft lithography as stamp resin, but a strong use is in biomedical microelectromechanical systems (bio-MEMS), in particular for microfluidics. There are also some application in flexible electronics thanks to the characteristics related to cost,

very low, fabrication, very easy, optical transparency and flexibility.

In figure 1.10 is shown a microfluidic analyzer that can analyze and measure biological

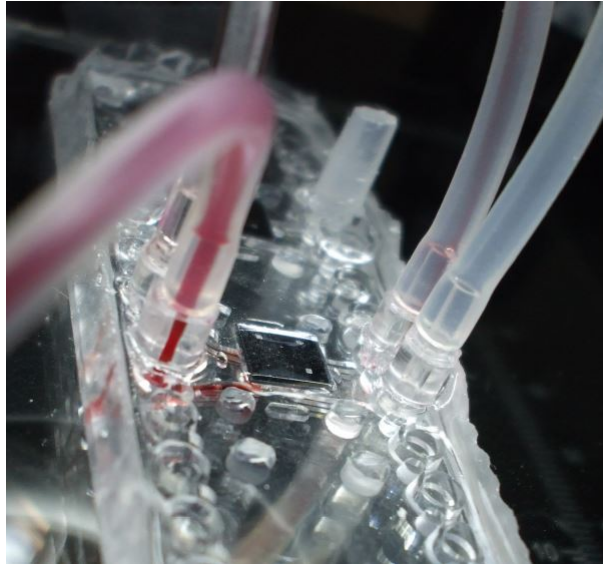


Figure 1.10: The developed microfluidic analyzer of Ref. [2] background system is able to analyze, measure biological liquids and calculate the number of morphological well-separated different elements with optical and electrical way.

liquids and it is able to calculate the number of morphological well-separated different elements with optical and electrical way [2]. In the fig. 1.10 one of the inlets shown is blood instead the other two are saline solution.

This analyzer, in fact, is made with PDMS silicon rubber as middle layer because the surface of PDMS can be treated in order to bind two sides made of glass or other materials [2].

BACKGROUND THEORY

In this chapter the background theory that is necessary to carry out the experimental part, located in chapter 3 and chapter 4 is treated.

In the first part of the chapter strain sensors are introduced and described explaining firstly the main figures of merit used to characterize them, as the gauge factor, secondly the different types and materials of strain gauges and finally some examples of applications are presented. There is a LIG strain gauges examples on polyimide described used for biomedical application.

In the second part of the chapter the supercapacitors (SCs) are introduced in general: the basic structures of SCs are described, in particular the conventional and the interdigitated one. Then the most often use materials for SCs are listed and described, focusing on the different elements in which the SCs are composed, such as electrolytes, electrodes, separators, etc.

Finally in the last section the measurements to evaluate the performances of this devices are described, focusing on cyclic voltammetry, electronic impedance spectroscopy and current constant charge/discharge.

2.1 Strain sensors

According to the definition provide by paper [17] strain gauges are electrical conductors whose resistance depends on their geometry. This change in resistance is usually measured by means of a Wheatstone bridge. More in general Strain gauge is a device used

to measure strain. The strain is a measure of deformation, where the deformation has units of length but strain is dimensionless and, as usual, it is expressed with percentage, decimal fraction or in parts-per notation.

In fig. 2.1 there is a basic scheme of a simple strain gauge.

In engineering Strain is called *engineering normal strain* and it is equal to the ratio

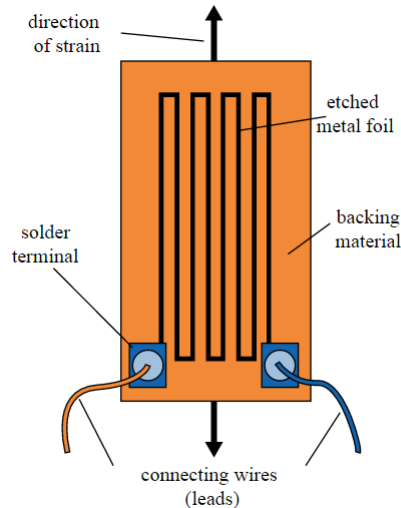


Figure 2.1: Basic scheme of a common type of strain gauges [21]

between $\Delta l/l_0$ where Δl represents the difference between l , the final length after an applied stress, and l_0 , the initial length.

Usually they are designed as long and thin conductive patterns, organized in a zig-zag configuration of parallel lines [21]. When this thin conductive pattern is stretched within the limits of its elasticity in order to avoid breaks or permanent deformations its electrical resistance increases. The opposite phenomena happen when it is compressed, it becomes shorter and broader decreasing its electrical resistance [21].

The use of a zig-zag pattern does not increase sensitivity, because in percentage the change in resistance is the same for a single line or for the entire zig-zag. The real advantage of this type of structure is to reduce overheating problems or to operate with higher voltage. Strain gauges provide high sensitivity, high repeatability, suitable also for small applications, for example fingertip [13].

They are easy to integrate in MEMS but often they are fragile so it is better to add some protective elastomers.

The basic working principle is the following: if the object is deformed, also the foil is deformed and this induces a change in the electrical resistance. This change is in relation with the mechanical stress ϵ by means of the gauge factor (GF) according to the equation

2.1:

$$(2.1) \quad GF = \frac{\Delta R/R_0}{\epsilon}$$

Typical values of GF for metallic foils range between 2 and 5, instead for semiconductor devices the GF is larger. One of the numerous advantages of SG is to have MEMS strain gauge, this implies easy integration in high-density devices but, on the other hand, there is an huge problem of fragility, low deformability and also there some difficult in packaging [17]. In order to overcome this problems strain gauges are often embedded into polymeric flexible substrates or simply covered by protective polymeric layer, in particular, thanks to his bio-compatibility, PDMS is often used [21].

A relatively recent evolution arrives with LIG, laser induced graphene (1.3) where there is the possibility to direct writing with a CO_2 laser onto a substrate in an atmosphere ambient.

Another drawback of strain gauges is the effects induced by variations in temperature. The first effect is related to the size that can change due to a thermal expansion that can be erroneously detected as a strain variation. In order to avoid this problem self-temperature compensation (STC) mechanism are used, selecting specific alloys [21].

When STC is not possible another compensation could be implemented by means of the dummy gauge technique. The basic principle is easy, this dummy element is put on unstrained sample which is in thermal contact with the sample with the active strain. This dummy element is wired in a Wheatstone bridge on the nearer contact of the active strain. Whit this technique is possible to that the effects induced by the temperature cancel each others.

The strain are attached to the sample by means of a glue that is chosen according to the required lifetime. A lot of precision must be achieved during the preparation of the surface, otherwise the strain measurements can result unreliable and unpredictable, causing errors. In order to avoid this the surface must be smoothed, deoiled with solvents, after the solvent removal the strain must be immediately glued to avoid undesired pollution [21].

2.1.1 Types and materials of strain gauge

The majority of strain gauge are made by a copper-nickel alloy called 'constantan alloy'. For measurements of small strain, the strain gauges are commonly made by semiconductor because there are a larger GF that it is reflected into a more sensitive device respect to temperature changes but also more fragile and expensive [21].

If there is the necessity of devices with high gauge factor, large deformation range and also small electrical consumption nanoparticle-based strain gauges are used made assembling conductive nanoparticles, for example gold or carbon [21].

Another type used in biological measurements is made with mercury-in-rubber, so a small liquid mercury inserted into a a tube of rubber [21].

Microscale strain gauges, already cited in the previous section, are widely used in MEMS to measure variation caused by pressure, sound, force or acceleration. There is also capacitive strain gauges that exploits the use of variable capacitors in order to derive the mechanical deformation.

Instead in civil engineering vibrating wire strain gauges are used measuring the resonant frequency of the wire in order to calculate the strain [21].

Recently, thanks to a new material LIG (introduced in section 1.3, strain gauges can be directly written onto a substrate exploiting the use of a pulsed CO_2 laser. In fact in the next section there is an example of an artificial throat made by LIG and polyimide.

2.1.2 Application of strain gauges

In literature there is already an example of an intelligent artificial throat with sound-sensing ability based on LIG onto polyimide [12]. This artificial throat can generate sound and also detect sound in a single device, the advantage of it compared to the others is that it is one-step fabrication (fig. 2.2), low cost, high efficiency and flexibility.

The artificial throat has the integrated functions of emitting and detecting sounds [12].

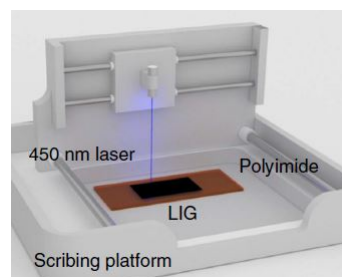
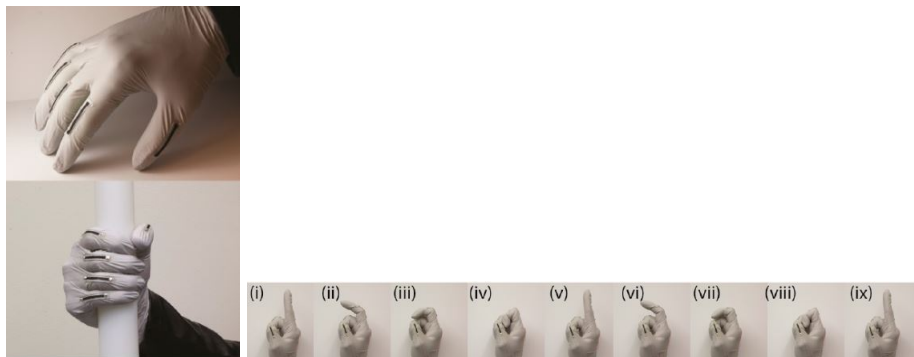


Figure 2.2: One-step fabrication of artificial throat made exploiting LIG [12]

The basic working principle of this device is the following: when an AC voltage is applied, the periodic Joule heat cause the expansion of air, that results in sound waves. However, if a low bias voltage is applied there will be a fluctuation in current due to the variation of resistance because of vibration of throat cords. Therefore, the devices can work as sound

source and detector at the same time. Thanks to its thermoacoustic and piezoresistive properties the LIG throat of Ref. [12] could be an excellent device.

Another application of strain gauges could be the one present in picture 2.3. In Ref. [16] there is a technique that is based on transfer carbonized patterns, obtained with laser pyrolyzation of thermoset polymers (e.g. polyimide), into elastomers, such as PDMS. The basic principle is quite simple. According to the finger bending, producing strain into the strain gauges, it is possible to evaluate the changes in resistance and from this, the angle of deflection is derived. It is very useful, for example, to control the motion of a robotic hand.



(a) Five stretchable strain onto a glove (b) Different bending stages of the strains onto the glove

Figure 2.3: Example of human finger motion detection with stretchable carbon traces [16]

2.2 What is a supercapacitor?

In this section supercapacitor are described, focusing on the different structures, the materials used and the different measurements for evaluate the SC performances are defined.

The starting point is that today batteries alone cannot be the only solution for electricity storage, mainly for three reasons. The first one is the low power density, because in some applications is required high power discharge and/or recharge rate and common batteries aren't able to achieve this task.

The second problem is related to the redox reactions in batteries that may lead to Joule heating during operation that must be dissipated, so heat generation is the other problem. The last one, the third main problem, is the cycle life because, in batteries, is limited.

In order to overcome these issues it is important to introduce supercapacitors, also called ultracapacitors or electrochemical capacitors. They mainly consist of two high surface area electrodes separated by an electrolyte. They demonstrate excellent reversibility, very long cycle life respect to batteries, less thermochemical generated heat outstanding power performance and easy integration in electronics. This is mainly due to the simpler charge storage mechanism it is possible to define two different charge storage methods:

- At the interface between capacitor electrode and electrolyte, as EDL (electric double layer) the charges are stored electrostatically.
- At the electrode surface as pseudocapacitance (PC) charges are faradaically stored.

An EDL is defined as a structure where two charged layers are formed at the electrode/electrolyte interfaces. The earliest model of EDL was defined by Helmholtz [6].

Pseudocapacitance arises when a faradaic charge transfer process occurs across the EDL. The consequence is a relation between the charge accumulated/released, that is potential dependent, and the capacitance.

Some hybrid capacitors exist which combine battery electrodes and capacitive electrodes form PCs and/or EDLs in order to obtain high power performance and improvements in energy storage ability, briefly described in the article [23].

A schematic diagram of the different types of capacitors is in fig.2.4. In particular supercapacitors that are fabricated by means of active carbon or graphitic carbon nanomaterials, as graphene or single-walled carbon nanotubes give the possibility to show their potential for attaining not only high energy but also power densities [9].

2.2.1 Supercapacitor structure

The conventional SCs are commonly assembled into button cells or in a spiral-wound configuration. The drawback of this kind of structure is that they are not flexible, bulky and heavy.

This conventional SCs (Fig. 2.5) is often composed in four main parts: current collectors, a separator, an electrolyte and electrode materials. These parts are usually packaged into a spiral-wound configuration by the shell or a sandwich [11].

However, due to the recent developments, the necessity of devices that are flexible, portable, thin, integrated comes out.

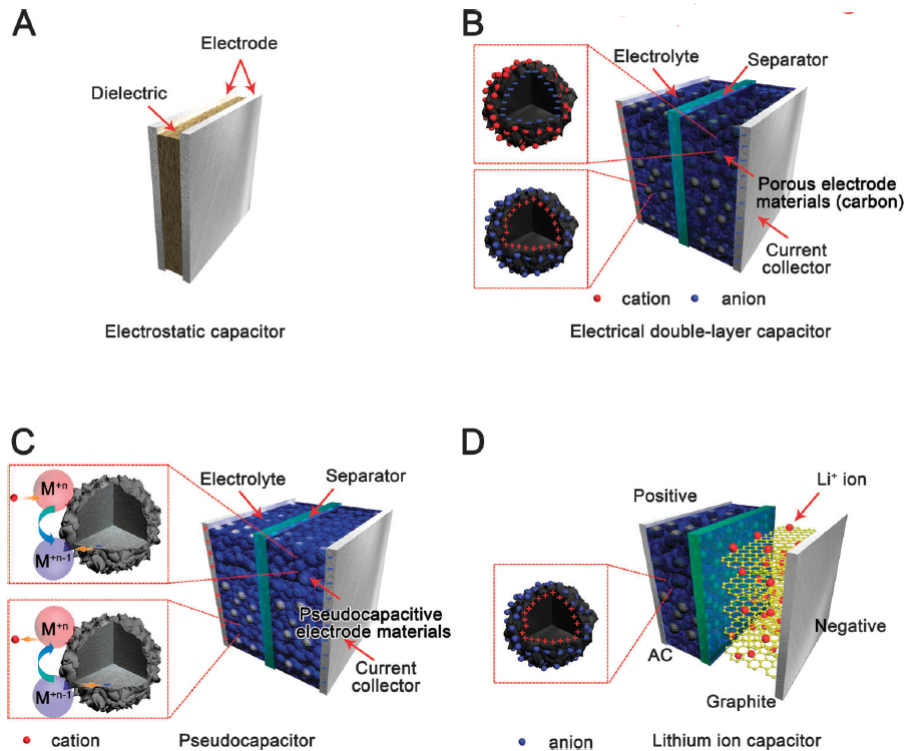


Figure 2.4: Schematic diagram of (A) electrostatic capacitor, (B) EDL capacitor, (C) PCs, (D) hybrid-capacitor [6]

To satisfy this demand another type of SCs consists in interdigitated electrode array, this type of structure results more compact and simplified respect the conventional one (Fig. 2.5).

They can bent without cracking and also its components such as electrode materials, current collector and the electrolyte can face to a strain quite high without remarkable losses in reliability and performances. An important aspect that must be underlined is that interdigitated SCs can be connected in series or in parallel on a single structure by means of the design of the structure of electrodes and the interconnection controlling the output operating voltage and the total capacitance. Instead 'bulky' SCs must be in parallel or series according to the external connection. [11]

2.2.2 Materials of SCs

Maintaining the division made in section 2.2.1 we can distinguish between conventional SCs structure and the one interdigitated. The electrodes of the first type are in general

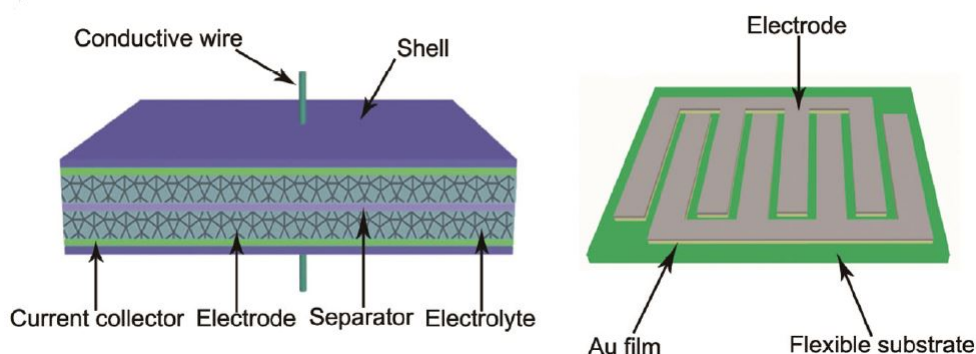


Figure 2.5: Schematics of conventional SC structure on the left side and of the interdigitated structure on the right side [11]

fabricated using a mix of active materials with conductive binders [11]. The next step consists in coating the composites on current collectors, as for example metal foil or foam. The active materials of conventional SCs are often active-carbon materials with their composites with transition-metal oxides/hydroxides and/or conductive polymers. The separator of conventional SCs is composed of porous polymer films and cellulose fiber papers.

For interdigitated SCs the active electrodes are usually made with materials with unique structures like graphene, carbon nanotubes (CNTs), carbide-derived carbon, nanostructured PEDOT, PANI and their composites. This particular structure does not need the separator because the space that there is between the fingers replace the physical separator. Instead the current collector is usually made by metal ultrathin films or in some cases the active material itself can work also as current collector [22].

The performances of these devices in main part depend onto the architecture but also the materials of the electrodes, optimum parameters for thickness, width and space between the electrodes have to be find.

In general electrolytes provide ionic conductivity on each electrode. They have a key role during:

- EDL, electric double layer, formation;
- Reversible redox process for the charge storage (in pseudocapacitors);

In the article [6] is present a classification of electrolytes used nowadays. There are divided into three big categories: in the first one are inserted the liquid electrolyte that

can be divided in two subgroups: aqueous and non-aqueous one, in the second one there are solid-state or quasi solid-state electrolyte, into the third one there are redox-active electrolyte.

Obviously different types of electrolytes have different range of potential windows. For example, the aqueous one have an operating potential window of about 1-1.2V.

In general, according to paper [6] the requirements for an ideal electrolyte are essentially:

- high chemical and electrochemical stability
- high chemical and electrochemical inertness to ES components
- low cost
- wide operating temperature range
- well-matched with the electrolyte materials
- wide potential window;
- low volatility and flammability
- environmentally friendly
- high ionic conductivity

According to the previous categories of electrolytes the organic solvents result more indicated for the conventional SC instead for the interdigitated one, which can also be subjected to bending, the gel one, aqueous based, result adequate. In this master thesis during the measurements the aqueous electrolytes used is 1M Na_2SO_4 .

2.2.3 Supercapacitor performance evaluation

The key parameters to characterized the performance of a supercapacitor is well described and standardized in article [23].

The most important parameters that must be evaluated and compared are cell capacitance, operating voltage, equivalent series resistance, power density, energy density and time constant. Nowadays inconsistencies and confusion exist because there are different methods and practices but the article [23] defines standard evaluation methods.

The sufficient parameters needed to compare commercial products fixing fabrication, materials and cell design are:

- Cell (total) capacitance C_T

- Operation Voltage V_O
- Equivalent series resistance R_{ES}

In research there is a large group of important factors taken into account in order to obtain a paint of the whole picture of supercapacitors due to the continuous new cell designs, advanced manufacturing process and a lot of additional factors.

A simple scheme (fig. 2.6), shown in Ref. [23], illustrate the key factors, performance test methods and metrics. There are different techniques or methods to characterize

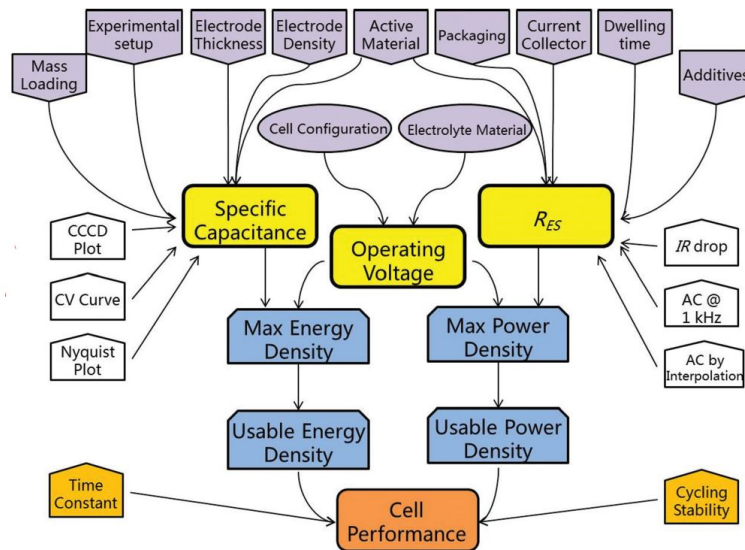


Figure 2.6: Scheme pf key performance test methods and metrics for evaluate SCs

the electrochemical performance of supercapacitors, the most common are cyclic voltammetry (CV), constant current charge/discharge (CCCD) and electrochemical impedance spectroscopy (EIS).

Thanks to them it is possible to evaluate time, voltage, current and the the other parameters can be evaluated from the three fundamentals. These other factors include capacitance, equivalent series resistance, time constant, energy and power.

It is very important to distinguish, from a technical point of view, between SC devices and SC materials, in order to make correct comparison. The difference between them is that SC devices include the whole package instead SC materials include only electrode and electrolyte materials.

The cycle-life is Another key parameters for measuring the ES performance. This is an indicator of the stability of the ES.

Following the stream of consciousness of the article [23] in this master thesis is used to characterize supercapacitors CV, CCCD and EIS. In paper [4] there is a review of calculation of capacitance, power and energy of EDLCs.

This calculation is performed under the assumption that the device behaviour is equivalent to a fractional-order circuit consisting of a resistance R_s in series with a CPE(Q, α), constant phase element in order to include nonlinear effects through the coefficient α . The expressions are present in the following subsections.

It is convenient to represent the behaviour of the electrode interphase with an equivalent simplified circuit, presented in fig.2.7.

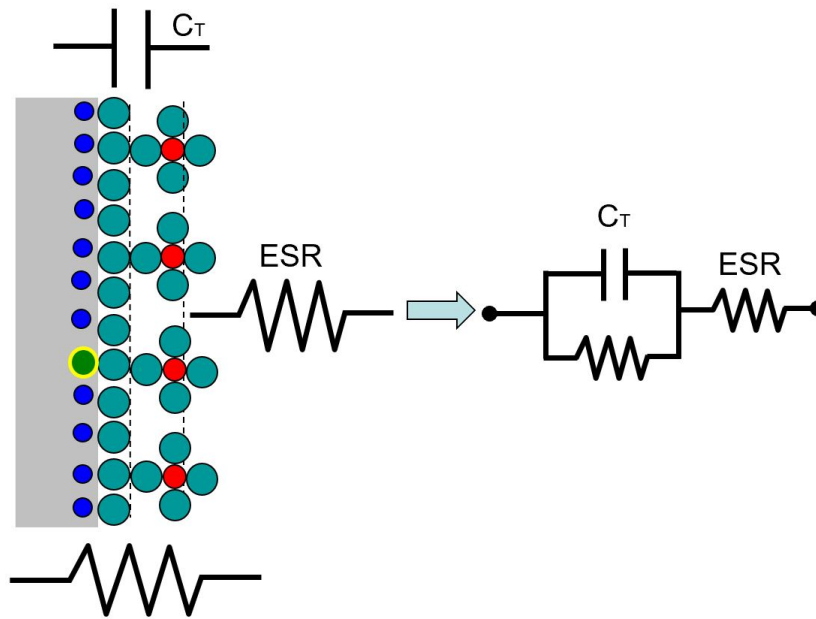


Figure 2.7: Simplified equivalent circuit of SCs

A basic electrical scheme is the series of a EDL capacitance with the solution resistance if it considers an ideally polarizable electrode. However Faradaic leakage currents have to be considered.

They arise depending on solution composition and electrode potential. These currents can be included in the scheme adding a 'Faradaic resistance' in parallel with the capacitance 2.7.

2.2.3.1 Cyclic voltammetry

In general, cyclic voltammetry is an analytical technique based on the measurement of the current flow through an electrode while a scanning potential is imposed to it. This electrode is called working electrode.

The use of this technique is the basis of comprehension of the laws concerning several electrochemical phenomena. In particular this test consists of applying a linearly changed

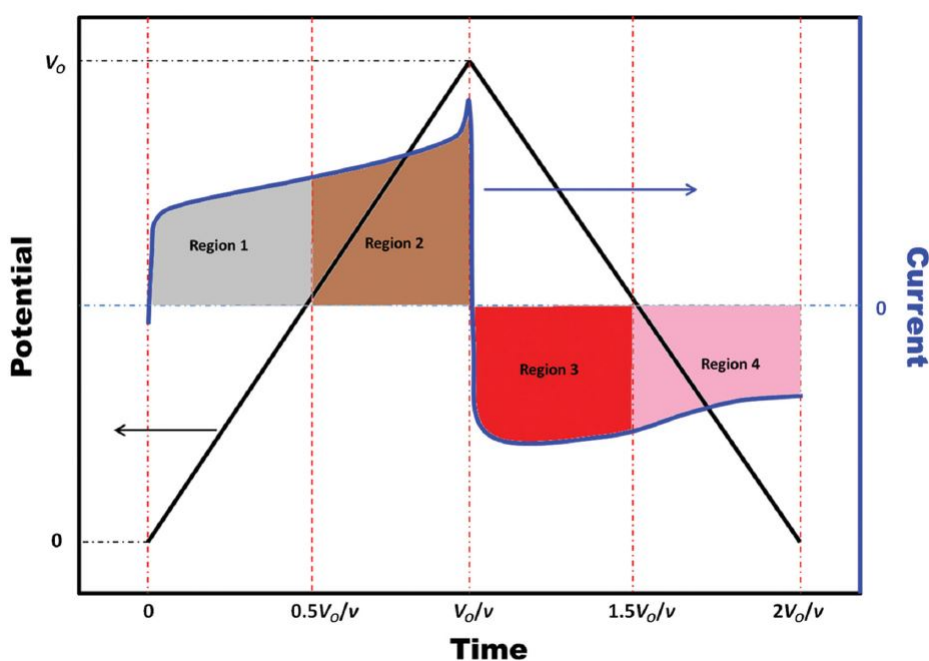


Figure 2.8: Typical CV, in black the potential applied, in blue the typical current plot obtained for a supercapacitor vs time [23].

electric potential between the two electrodes 2.8, the positive and the negative one in the case of two electrode systems. However for a three-electrode system configurations the electric potential is applied between reference and working electrodes.

In this measurements the scan rate(v) expressed in mV/s measures the speed of the potential change instead the range of the potential change is called operating potential or potential window. The current is recorded and data obtained are plot in cartesian graph of Current(A) vs. Voltage(V).

Thanks to the shape of the obtained plots is possible to distinguish between EDLC or PC materials. Integrating the CV curves is possible to obtain the integral capacitance C of the target electrode from eq.2.2:

$$(2.2) \quad C = \frac{1}{\Delta V(dV/dt)} \int I dV$$

where dV/dt is the voltage scan rate and the numerical integration of the current is over half-cycle potential ΔV . The storage energy is evaluated from $E=C\Delta V^2/2$ and the power (P) from $P=V^2/4R_S$ assuming an ideal capacitive behaviour. For pure voltage-independent capacitive behaviour the current is linear with the voltage sweep rate (ν) and the voltammograms are ideal rectangles with mirror-image symmetry with respect to the zero current axis [4]. A non ideality is the increase of positive slope of voltammetric current responses that increase increasing ν .

2.2.3.2 Constant current charge/discharge

This technique consists in a repetitive charge/discharge of the SC device keeping a constant current level 2.9. The output plot is a cartesian graph with the potential in the y axis and the time in the x axis. All the three core parameters (C_T, R_{ES}, V_O) can

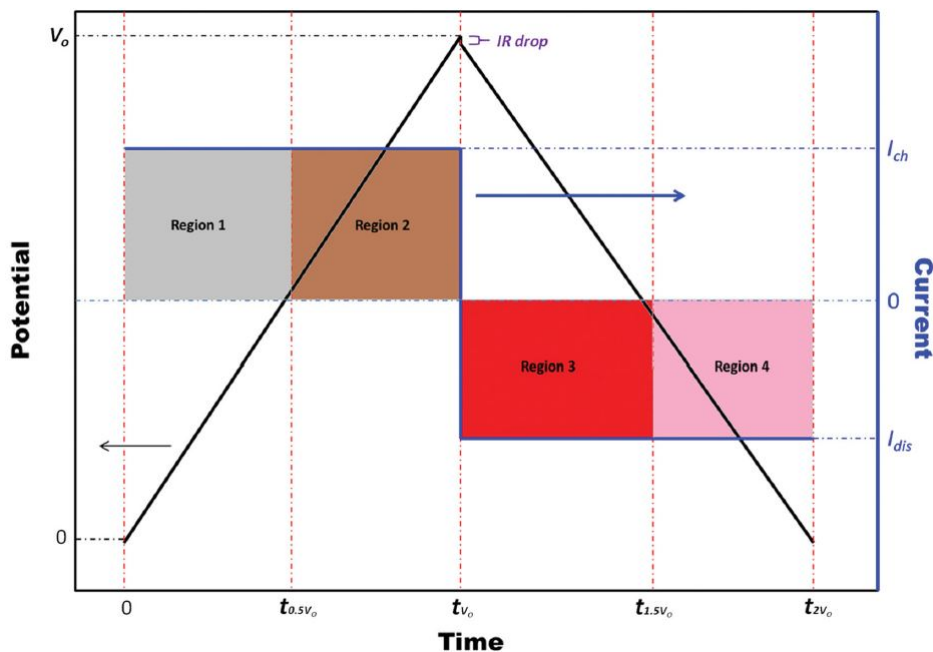


Figure 2.9: Typical CCCD, in blue the current imposed, in black the typical potential vs time plot obtained for a supercapacitor [23].

be tested, also for deriving the other secondary parameters. During a galvanostatic charge/discharge, that is a study of the transient voltage response when is applied a

stepping current I_{CC} , is possible to evaluate from eq.2.3 the average capacitance:

$$(2.3) \quad C = \frac{I_{CC}}{dV/dt}$$

where dV/dt is the slope of time-voltage curve [4]. In ref.[4] there is a review in the calculation of capacitance, power and energy of EDLCs from the time domain constant-current step response and linear voltage waveform. The background assumption is that the device behaves as an equivalent fractional-order circuit consisting of a resistance R_s in series with a constant phase element $CPE(Q, \alpha)$, where Q is a pseudocapacitance and α is the dispersion coefficient [4]. They show with the derived (R_s, Q, α) -based expressions, that the corresponding nonlinear effects in voltage-time and current-voltage can be encompassed through nonlinear terms function of the coefficient α . This is not possible with the classical R_sC model [4]. The $R_s - CPE(Q, \alpha)$ model offers one extra degree of freedom respect to common R_sC model. When the impedance $Z(s) = R_s + 1/Qs^\alpha$ is excited by an input current step of amplitude $I_{CC} > 0$ the output voltage is given by eq.2.4:

$$(2.4) \quad V(s) = \frac{V_0}{s} + \frac{I_{CC}}{s} \left(R_s + \frac{1}{Qs^\alpha} \right)$$

Re-arranging:

$$(2.5) \quad V(s) = \frac{V_0}{s} + \frac{I_{CC}}{s} \left(\frac{R_s}{s} + \frac{s^{-1}}{Qs^\alpha} \right)$$

Applying the inverse Laplace transform as paper [4] describe in details, the voltage-time characteristics of an $R_s - CPE$ equivalent model is obtained 2.6:

$$(2.6) \quad V(t) = V_0 + I_{CC} \left(R_s + \frac{t^\alpha}{Q\Gamma(1+\alpha)} \right)$$

If we consider an ideal capacitor with $\alpha = 1$ and $Q=C$ in Farads the equation obtained substituting in 2.6 is 2.7:

$$(2.7) \quad V(t) = V_0 + I_{CC} \left(R_s + \frac{t}{C} \right)$$

CCCD is useful to study the cycling stability.

2.2.3.3 Electrochemical impedance spectroscopy

EIS applies a low-amplitude alternative voltage superimposed on a steady-state potential in order to obtain the impedance of a power cell as function of frequency. The graphs

obtained from this study are Bode and Nyquist plots. With the first one the cell response between the phase angle and the frequency is been evaluated. From the second one, the Nyquist plot, the cell impedances on a complex plane is shown. The real part of the complex impedance at a certain frequencies represents the R_{ES} , equivalent series resistance ([4]). Thanks to EIS is possible to evaluate charge transfer, mass transport,

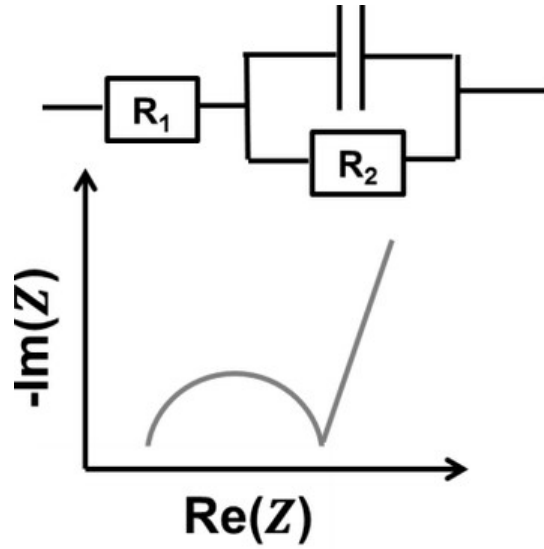


Figure 2.10: Example of Nyquist plot for the circuit represented in figure.

capacitance, energy and charge storage mechanisms. In the frequency domain, EDLCs have a constant phase or fractional power characteristics different from the response of an ideal capacitor [4]. It's common that the Nyquist plot shows non linear behaviour with more deviation from ideality like semi-circle due to non-perfect coulombic phenomena, inclined pseudo-Warburg region. EIS is a powerful tool to obtain the equivalent electric circuits of dynamic processes but the frequency response is quite expensive from hardware and software point of view [4], in fact it's possible to extract it from CCCD and CV using fractional-order calculations as previous described.

2.2.3.4 Capacitance, energy density and power density

As shown in fig.2.4 the entire ES can see as two capacitors in series because electrode/electrolyte interfaces represent a capacitor. The total capacitance of a SC is defined as $C_T = \Delta Q / \Delta V$, so the electrical charge stored under a given voltage change. C_T is used more with an SC device instead for SC materials is better to use C_S that is equal to C_T / Π where Π can be the mass, volume, surface area or the size of the electrode. Returning to

the total capacitance, it can be expressed by the eq.2.8:

$$(2.8) \quad C_T = \frac{\Delta Q}{\Delta V} = \frac{\int_0^{2V_0/v} \|i\| dt}{2V_0}$$

The theoretical energy density of the ES cell can be expressed by eq.2.9 and the power density by eq.2.10:

$$(2.9) \quad E = \frac{1}{2} C_T V^2$$

$$(2.10) \quad P = \frac{1}{4WR_{cell}} V^2$$

Where R_{cell} is the equivalent series resistance. It's evident from eq.2.10 that power density increases with a decreasing R_{cell} value. Equivalent series resistance, as defined in paper [6] is the total sum of different types of resistances including intrinsic resistance of mass transfer resistance of the ions, the electrode material and electrolyte solution and contact resistance between the electrode and the current collector.

LASER WRITING SET UP & MATERIAL CHARACTERIZATION

This chapter is mainly divided into four parts: the first one gives a general description of the CO_2 laser used to obtain LIG patterns. In particular the parameters that has been used were analyzed in order to find the optimum laser writing procedure. Then there is a description of the laser system used to perform the writings analyzed and characterized in this master thesis. At the end of the this first part the geometries used in this master thesis are inserted, the one of strain sensors and supercapacitors.

The second part has the aim of finding the best parameters of writing in order to perform a complete characterization. This one starts with the analysis of conductivity of LIG onto different substrates by means of Sheet Resistance parameter. Current/voltage characteristics were recorded with an inline two-point probe configuration using a Keithley 2635A source measure unit.

The next step was to find conductive patterns on pure PDMS because the chemical and electrical properties change completely compared to the polymers present in literature [22]. To improve the conductivity of materials a successful technique was to add triethylene glycol (TEG) into PDMS matrix. Then in order to find a specific trend and variation of conductive parameters the percentage of TEG into PDMS is varied from 10 % to 40 % in weight. Overcome this limit of percentage is not possible because TEG does not dilute more into PDMS.

In literature [22] materials with Aramide are already successfully used and a conductive

analysis is carried out also onto this substrates.

Another section focus onto an analysis of the obtained LIG patterns, exploiting the use of Scanning Electron Microscopy (SEM), Raman spectroscopy and XPS elemental analysis, techniques explained in detail in section 3.3.

In the final section mechanical tests to determine the Young's module of these various substrates are performed using a machine able to stretch the materials until reach the break point.

3.1 Laser description and operation

In general laser is an acronym that stands for light amplification by stimulated emission of radiation.

The laser used to write on PDMS is present in fig.3.1. It is a pulsed-laser CO_2 with 10064



Figure 3.1: Laser CO_2 present in Microla Optoelectronics laboratory in Chivasso
nm of wavelength, the maximum power is 30W that is subdivided by the software in

percentage ranging from 1 to 100. It exploits the use of a galvanometric head in order to address the laser beam, it has two mirrors able to move at a velocity that vary from 5 to 6000mm/s.

Screwed the galvanometric head there is a Teta lens of 100mm, this is defined the maximum available work field of 70X70 mm and a final spot between 270 and 300 μm . The software used is 'Lighter'. The laser has an autofocus equipped with a instrument, that measure the distance, called 'Keyence', a preview is available in order to locate in the correct position the laser writing, external hoover to absorb the smokes produced.

3.1.1 Parameters variation

In this type of CO_2 laser system the laser parameters that it is possible to set are the power, the frequency, which defined the length of the period, the pulse width, that defined the number of the pulses inside the period and the repetition. Wobble is another option available which consists in writing in a 'circular way'. It is possible to write area instead of lines, in this case the filling procedure must be selected. The area is written using single lines, crisscross lines oriented with specific angles that can be set.

The distance between lines must be chosen, defined as interline expressed in mm, the direction of writing could be unidirectional or bidirectional. During the laser writing performed these key four parameters have been changed. Normally power is varied, for the substrate used in this master thesis from 1 % to 5 %, otherwise, if it is increased above this level it can puncture the substrates. The frequency is kept often stable to 10 kHz. Instead the velocity is often changed according to the power. A trade-off between the two parameters is found but often the velocity range from 5 mm/s to 125 mm/s. Then the number of repetition is essential to allow the LIG formation onto PDMS substrates. As already described in Ref. [22] multiple laser passes in polymer substrate can permit the conversion of the material into LIG.

3.1.2 Geometries

The geometries used are:

- Lines with a length of 15mm
- Strain sensors with 3 different shapes varying the length (fig.3.7b)
- Supercapacitor with 10 interdigitated fingers, 25mm long and 12mm wide (fig.3.7a).

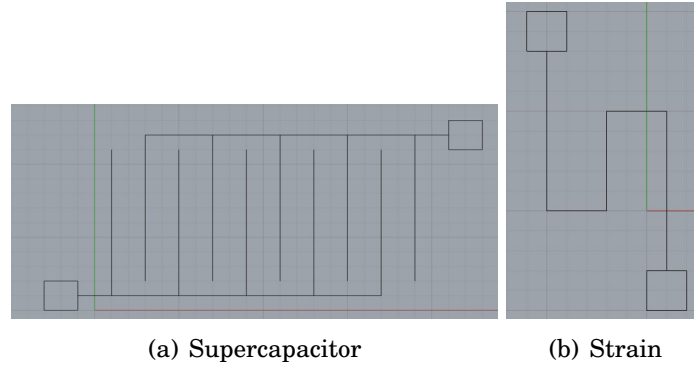


Figure 3.2: Geometries designed with Rhino 6 CAD software used in laser writing, each square of the grid is 1X1mm

3.2 Characterization of substrates

The aim of this section is to find the best writing parameters in order to perform a complete characterization. This last one starts with the analysis of conductivity of LIG onto different substrates.

The next step was to find conductive lines on pure PDMS because the chemical and electrical properties change completely and conductive areas in order to write contacts. Then Scanning Electron Microscopy (SEM), Raman spectroscopy and XPS elemental analysis are used with different purposes, explained in detail in section 3.3.

To analyze the conductivity, according to literature, the Sheet Resistance (R_S) is used as figure of merit. The R_S is defined as a measure of resistance used especially with thin films uniform in thickness. It is very commonly used because with this measure is possible to compare device with different sizes. In a regular three-dimensional conductive medium, which is long 'L', wide 'W' and thick 't', the resistance in general is defined as in equation 3.1, where ρ is the resistivity.

$$(3.1) \quad R = \rho \frac{L}{Wt}$$

Combining the resistance and the thickness the R_S is obtained:

$$(3.2) \quad R_S = R \frac{W}{L}$$

It is measured in ' Ω/sq ' or ' Ω/\square '.

A two-point probe configuration exploiting the use of a Keithley 2635A source measure unit permits to record the current/voltage characteristic in order to derive the Resistance

and then the Sheet Resistance. The contacts are made using silver conductive paint mono- and bi-components provided by RS PRO.

3.2.1 LIG lines on PDMS substrate

In this section an analysis of the conductive LIG patterns onto pure PDMS is performed. The PDMS used was 10:1 thanks to the properties explained in section 1.4.

The aim is to increase as much as possible the conductivity playing with the laser writing parameters. The parameters that have been changed to find best results are frequency (kHz), power expressed in percentage, velocity (mm/s) and number of repetitions. The multiple laser technique was already described in Ref.[22] and it allows enhancement of electrical properties because it increases the quality of LIG obtained.

In table 3.1 are listed the best parameters found in ambient conditions exploiting the use of the laser of chapter 3.1. The R_S evaluated from the laser writing with the parameters

Table 3.1: Working parameters of laser writing

Name	Geometry	Freq(kHz)	Power(%)	Velocity(mm/s)	n° of Repetitions
a	line 15mm	10	5	5	2
b	line 15mm	10	5	5	3
c	line 15mm	10	5	5	4
d	line 15mm	10	2	20	3
e	line 15mm	10	3	20	3
f	line 15mm	15	1	20	2
g	line 15mm	15	2	20	2

of table 3.1 is plotted in fig.3.3.

The values obtained are quite high so the purpose of this master thesis is to reduce the R_S in order to increase as much as possible the conductivity of the LIG patterns without compromising the extraordinary properties of pure PDMS (Section 1.4).

In literature [15], one of the improvements tested regards the creation of an inert ambient, with Nitrogen, in the chamber where the substrate is written [22].

The presence of Nitrogen seems to increase the conductivity of the LIG patterns.

A reduction in R_S is evident from the plots of fig.3.4 using Nitrogen. In fig.3.4 4 lines made with identical laser parameters are circled, 2 written in ambient atmosphere and 2 in ambient conditions.

It is evident that with Nitrogen the R_S is reduced. This is not enough, better results are

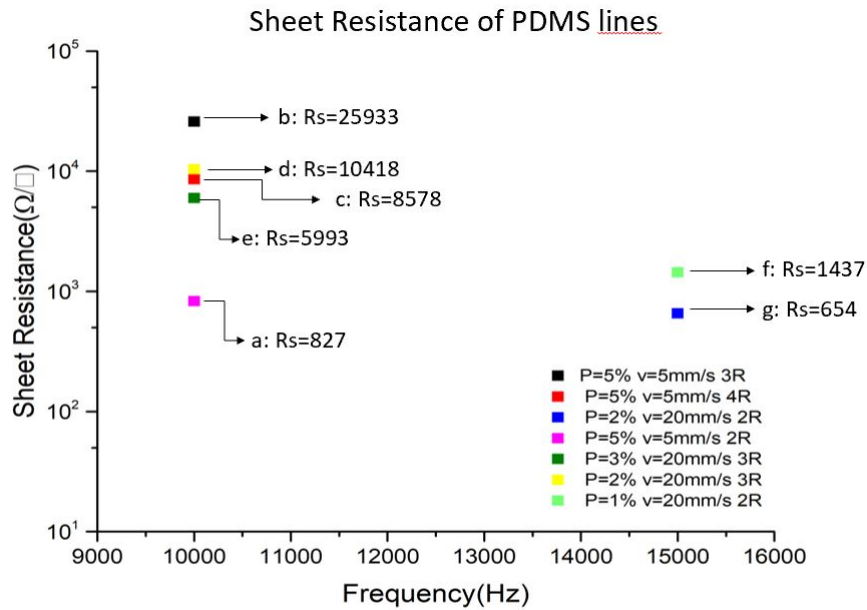


Figure 3.3: Plot of Sheet Resistance vs Frequency varying laser parameters according to table 3.1

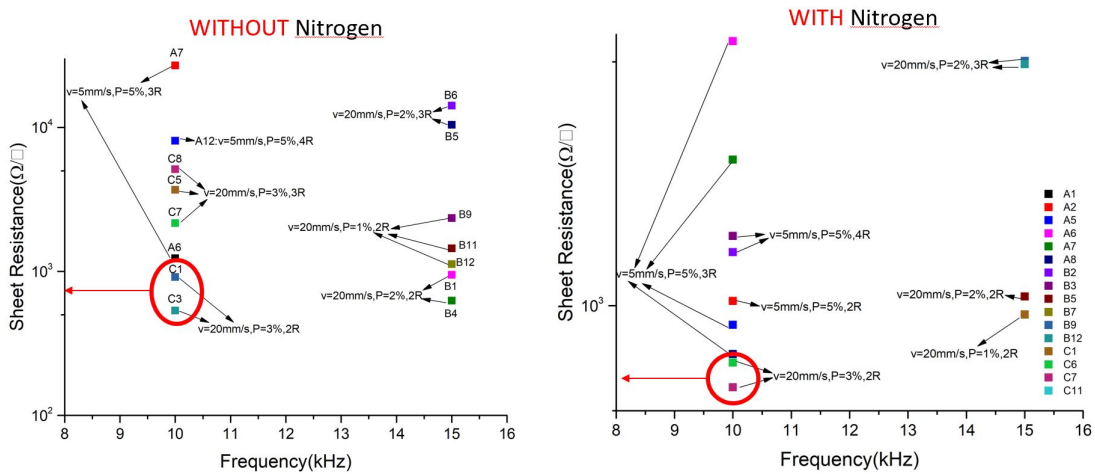


Figure 3.4: Comparison between Sheet Resistance of the PDMS lines written in inert ambient (Right fig.) or no (left fig.)

reached in section 3.2.2.

Due to these previous results in Sheet Resistance, in order to improve the conductivity of the lines some mixture of PDMS with other substances were tested to enhance the Carbon inside the structure. An addition of Aramide, C vitamin, Boro (B) (as shown in Ref. [25]), Polyethylene glycol (PEG), triethylene glycol (TEG), carbon fibers. The best results obtained are with the addition of TEG (section 3.2.2).

3.2.2 LIG lines on PDMS-TEG substrate

In order to improve the conductivity of LIG patterns on PDMS a lot of different substance were added to it and tested. The best mixture obtained is with triethylene glycol (TEG) inserted into PDMS in-weight in different percentage.

It is right, before describe the analysis of PDMS-TEG lines, present a little resume of TEG characteristics. TEG is viscous liquid that is colorless and odorless. It is more dense than water. It is used for vinyl polymers as plasticizer and its chemical formula is $C_6H_{14}O_4$. It is a poly(ethylene glycol), also known as PEG, in which the atoms of Carbon present in position 3 and 6 have been substituted with atoms of oxygen. Its main applications are in table 3.2, provided by [7].

Table 3.2: Main applications of TEG [7]

Hygroscopicity	Dehydration of natural gas Moisturizing and plasticizing cork, adhesives adhesives
Plasticizer	Safety glass Separation membranes (silicone rubber, polyvinyl acetate) Ceramic materials (resistant refractory plastics, molded ceramics)
Low Volatility Solvent	Gas dehydration Resin impregnants and other additives Steam-set printing inks Aromatic and paraffinic hydrocarbons separations Cleaning compounds Polyethylene terephthalate production equipment cleaning Cyanoacrylate and polyacrylonitrile
Chemical Intermediate	Unsaturated polyester resin Various resins of the alkyd type used as laminating agents in adhesives Esterification products used in plasticizer intermediates for nitrocellulose lacquers and vinyl resins Polyester polyols for polyurethanes Thermoplastic polyurethanes Silicone compounds Emulsifiers Lubricants
Freezing Point Depression	Heat transfer fluids

When it is inserted into the PDMS matrix the result structure seems to be like pure PDMS but the resulted color is more opaque and it tends to an ivory colour. In particular to define a specific trend TEG is inserted into PDMS in 10%,20%,30%,40% by-weight.

It is not possible to overcome 40 % because TEG does not dilute into PDMS. Looking to section 3.3.3 it is evident that increasing the percentage of TEG the resulted mixture is a little more elastic according to the Young's module, although this variation is not so preponderant.

The plot in fig.3.5 shows a specific trend: it is clear that the sheet resistance decreases increasing the amount of TEG into PDMS.

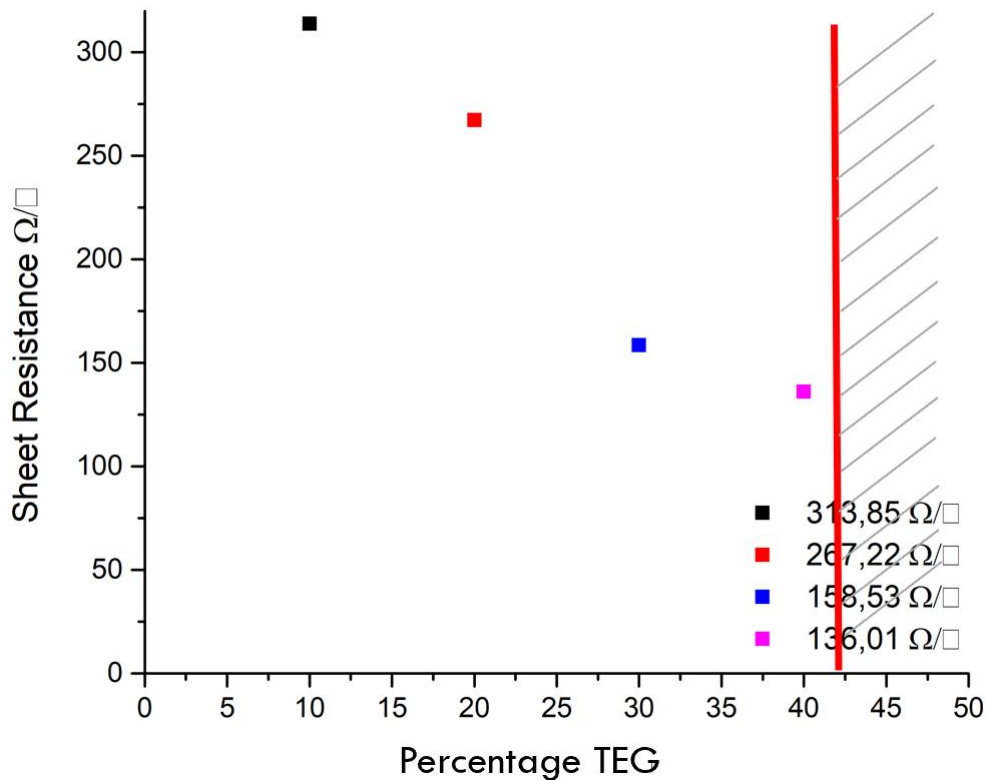


Figure 3.5: Trend of R_S increasing the percentage of TEG into PDMS

From fig. 3.5 it is possible to underline the fact that respect to the value of R_S of fig. 3.3 and fig. 3.4 the R_S goes down to $136\Omega/\square$, a huge improvements. Thanks to this promising results the mixture PDMS-TEG is used also to study devices, like supercapacitors and strain, in chapter 4 to enhance properties.

3.2.3 LIG lines on different substrates

A textile factory gave different types of tissues made with Aramide and also pure para and meta Aramide, the second one common know also as the commercial name Kevlar. A laser writing test onto a mixture of PDMS-KEVLAR is herein presented because in Ref. [22] this material is inserted in the list of working polymer tested.

The aim is to find huge improvements respect to previous matrix of pure PDMS and PDMS-TEG. In general, Kevlar is a synthetic fiber developed at DuPont, the aspect is a sort of fabric sheets that can be inserted into composite material components.

The matrix tested has a simple composition. Fabrics of Kevlar are linked together using PDMS, it is poured into the mould and put into an oven to solidify.

In fig. 3.6 a plot of Sheet Resistance vs Frequency is shown, the lower value of R_S is obtained with the line made also with Kevlar, reaching values of $83.52\Omega/\square$, $66.96\Omega/\square$ and $78.77\Omega/\square$. The problem regarding this substrate is that the mechanical properties changed completely, the flexibility is lost compared to the mixture PDMS-TEG that does not compromise it.

However the main problem of this mixture is that Kevlar was added into PDMS, not as a molecule, but in fibers, because the process to develop a composite of PDMS-Kevlar is quite long. It could be studied as possible material to obtain LIG patterns with high conductivity but this master thesis focus onto the analysis of improvements obtained by means of TEG addition.

Due to this conclusions other tests and improvements are not carried out in this master thesis. Thanks to the good results with PDMS-Kevlar mixture, in this section the conductivity of LIG lines written onto different substrates are tested. These tissues contain Aramide, base of Kevlar, in different percentage and they maintain their flexibility because of the mixture with other substances. The best results are obtained from the substrate of fig.3.7.

The laser parameters of writing are inserted in table 3.3 with reference to the pictures 3.7.

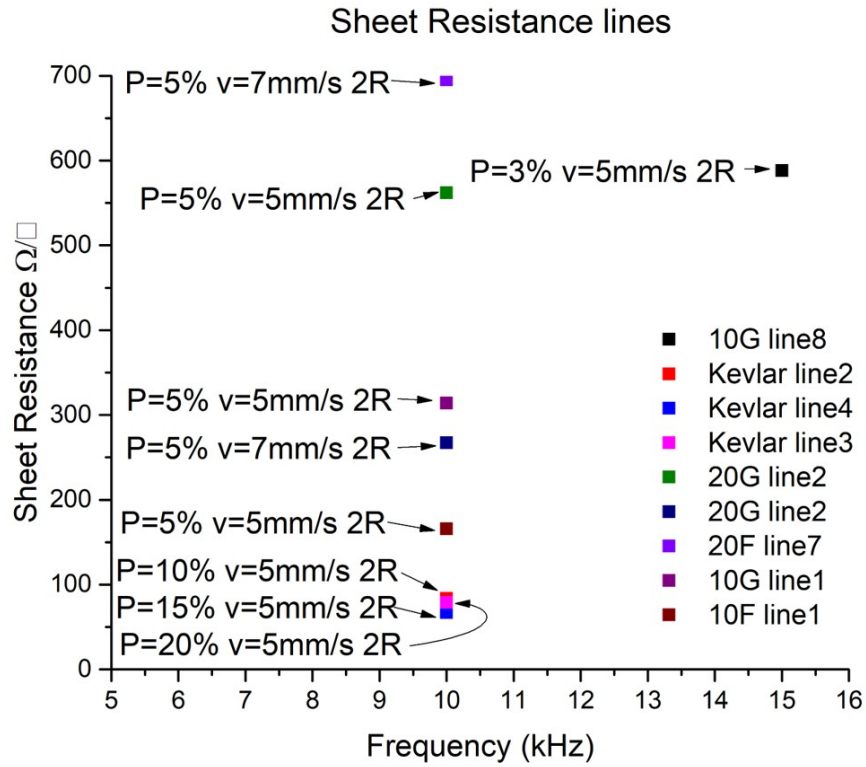


Figure 3.6: Comparison between lines written onto a substrate, made of a mixture of PDMS and TEG, and another substrate, made of a mixture of PDMS and KEVLAR

In this section that regards the characterization of the laser writings.

The best laser writing on substrate called 'ice' is line 4 with a R_S of $46.6 \Omega/\square$, bending test are inserted in section 4.1.3.

Instead onto the 'red' substrate the R_S of line 4 is approximately double respect to line4 of substrate 'ice', reaching $90 \Omega/\square$.

Then onto substrate called 'orange' the line 1 is the best one with a R_S of $81.2\Omega/\square$, bending test are inserted and plotted in section 4.1.3.

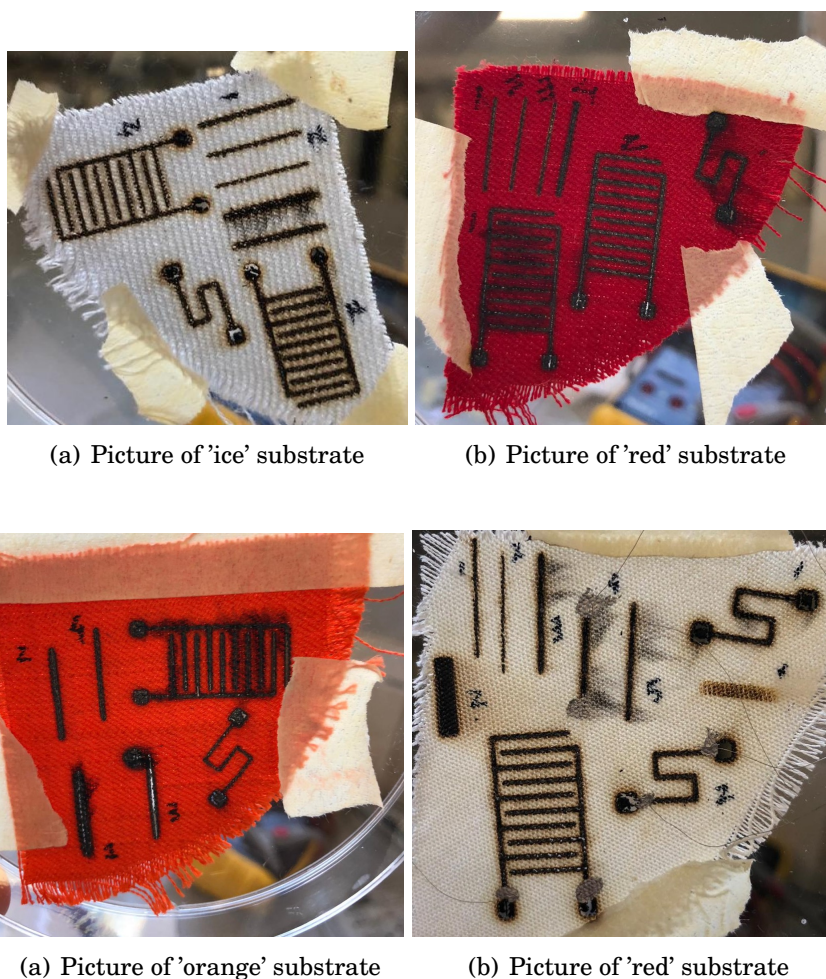


Figure 3.7: Pictures of the substrates made of percentage of Kevlar specify in the text

3.3 Raman Spectroscopy and Scanning electron microscope

In this section the LIG patterns obtained onto PDMS, PDMS-TEG mixture are analyzed with two different techniques. The first one treated is Raman spectroscopy (3.3.1) and the second one is Scanning electron microscope (3.3.2).

3.3.1 Raman Spectroscopy

The spectroscopy technique used to provide a structural fingerprint in order to identify molecules is Raman Spectroscopy.

Table 3.3: Working parameters of laser writing

Substrates	Name	Geometry	Freq(kHz)	Pw(%)	Vel(mm/s)	n° of Rep
Ivory	1	line	10	5	15	1
Ivory	2	line	10	5	20	1
Ivory	3,4	line	10	5	15	2
Ivory	5	line	10	5	20	2
Ivory	a	Strain	10	5	20	2
Ivory	b	Strain	10	5	10	2
Ivory	/	Supercap	10	5	10	1
Ice	1	line	10	5	10	1
Ice	2	line	10	5	15	1
Ice	3	line	10	5	20	1
Ice	4	line	10	5	10	2
Ice	5	line	10	5	15	2
Ice	/	Strain	10	5	10	1
Ice	a	Supercap	10	5	10	1
Ice	b	Supercap	10	5	15	1
Orange	1	line	10	5	5	2
Orange	2,3	line	10	5	10	2
Orange	1	line	10	5	15	2
Orange	/	Strain	10	5	15	1
Orange	/	Supercap	10	5	15	2
Red	1	line	10	5	15	1
Red	2,3	line	10	5	20	1
Red	4	line	10	5	15	2
Red	a	Supercap	10	5	20	1
Red	b	Supercap	10	5	10	1
Red	/	Strain	10	5	25	2

It exploits the use of a laser light to interact with molecular vibrations, phonons of the samples analyzed to obtain an analysis of the materials.

Renishaw InVia Reflex micro-Raman spectrometer equipped with a cooled CCD camera is used to obtain the plot of fig. 3.9, 3.8 and 3.10.

A parameter to indicate the degree of crystalization of the structured layer is the intensity ratio defined as the ratio between the D and the G peaks. Respectively the peak D is the one connected to the formation of defects, vacancies and bent sp² bonds and the peak G is the one born from the first-order inelastic scattering process [1].

Common features of few-layer of graphene are extrapolated from fig. 3.9, 3.8 and 3.10. First one is the D peak at approximately 1350 cm^{-1} . Then the G peaks are also evident

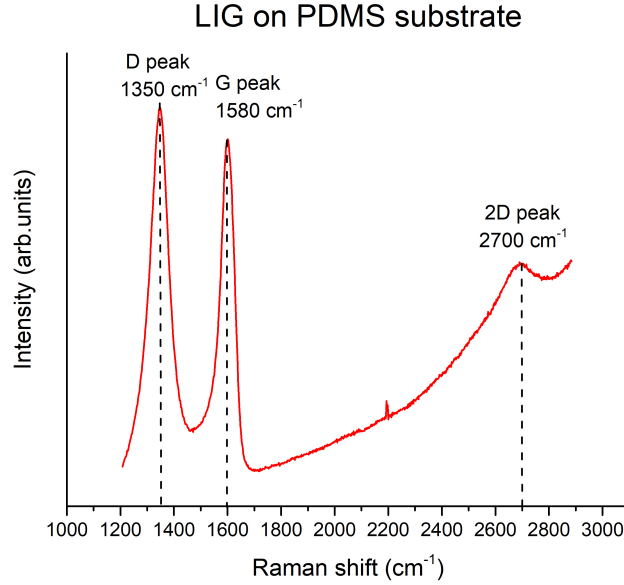


Figure 3.8: Raman of LIG on PDMS

at 1580 cm^{-1} in all plots. However the 2D peak at 2700 cm^{-1} is not very protruding and it is the second harmonic of the D band.

In fig. 3.8 the Raman characterization of LIG onto pure PDMS is plotted. The intensity ratio is equal to (1.07 ± 0.05) .

In fig. 3.9 4 figure showing the Raman characterization of LIG onto PDMS-TEG substrates in different percentage are represented.

Fig. 3.9a shows the Raman characterization of LIG onto PDMS-TEG 10% and an intensity ratio of (1.06 ± 0.07) is obtained comparing the 2 peaks.

Fig. 3.9b shows the same plot but for a percentage of TEG into PDMS of 20% with an intensity ratio of (1.36 ± 0.04) .

The highest ratio obtained is in picture 3.9c, related to PDMS-TEG 30%, and it is equal to (1.58 ± 0.08) .

The last image, the fig. 3.9d, plot the Raman of LIG onto PDMS-TEG 40%, the intensity ratio is also here quite high, (1.48 ± 0.05) .

In fig. 3.10 a comparison between the Raman characterization of LIG onto PDMS and onto PDMS-TEG 40% is shown. From the plots it is clear that the one of pure PDMS is less rich of defects. Infact there is not a big different between the D and G peaks. It is not possible to comment the same thing for PDMS-TEG where there is a huge difference

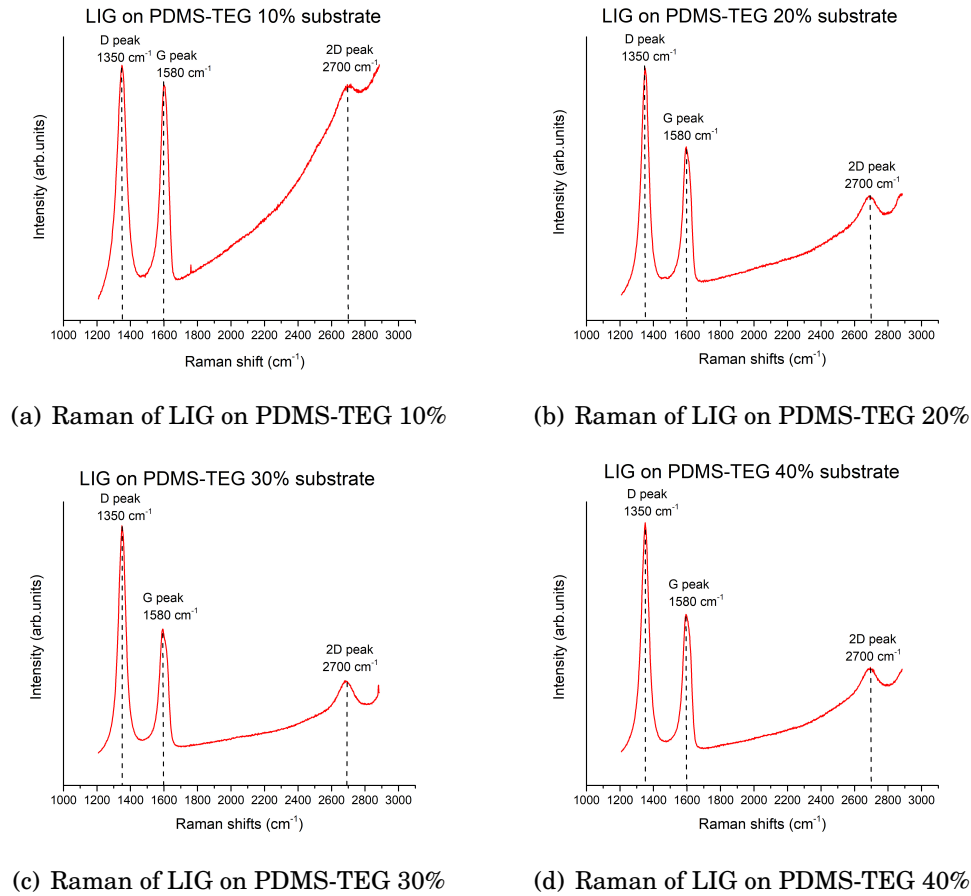


Figure 3.9: Raman of characterization of LIG onto PDMS-TEG in the 4 different % presented in section 3.2.2

as a matter of fact, the intensity of the D peak is doubled compared to the G one. Finally the I_D/I_G ratio analyzed from the different Raman spectra is quite high in PDMS-TEG substrates, so there is a quite high amount of defects in the graphitic materials.

3.3.2 Scanning electron microscope

The morphology of different LIG patterns onto pure PDMS and PDMS-YEG substrates was studied with a Zeiss Supra 40 field-emission scanning electron microscope that is equipped with an Oxford Si(Li) detector for energy dispersive x-ray analysis (EDX).

Thanks to Scanning electron microscope (SEM), it is possible to obtain images of sample when the surface is scanned by means of a focused beam of electrons.

In fig.3.11 there are 4 FESEM picture of PDMS-TEG LIG lines varying the percentage of

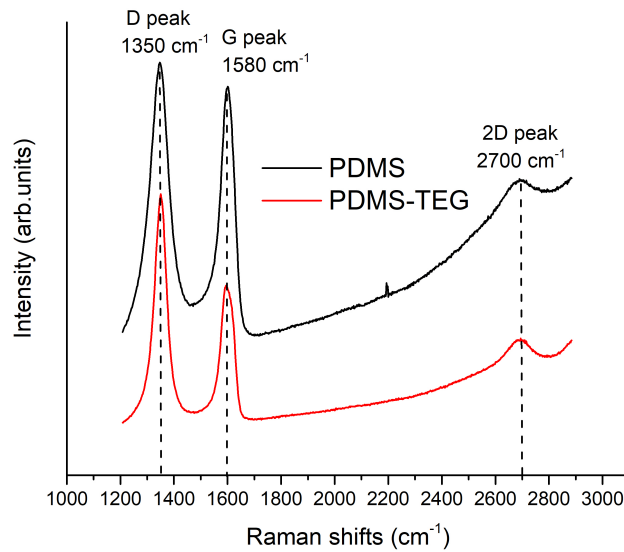
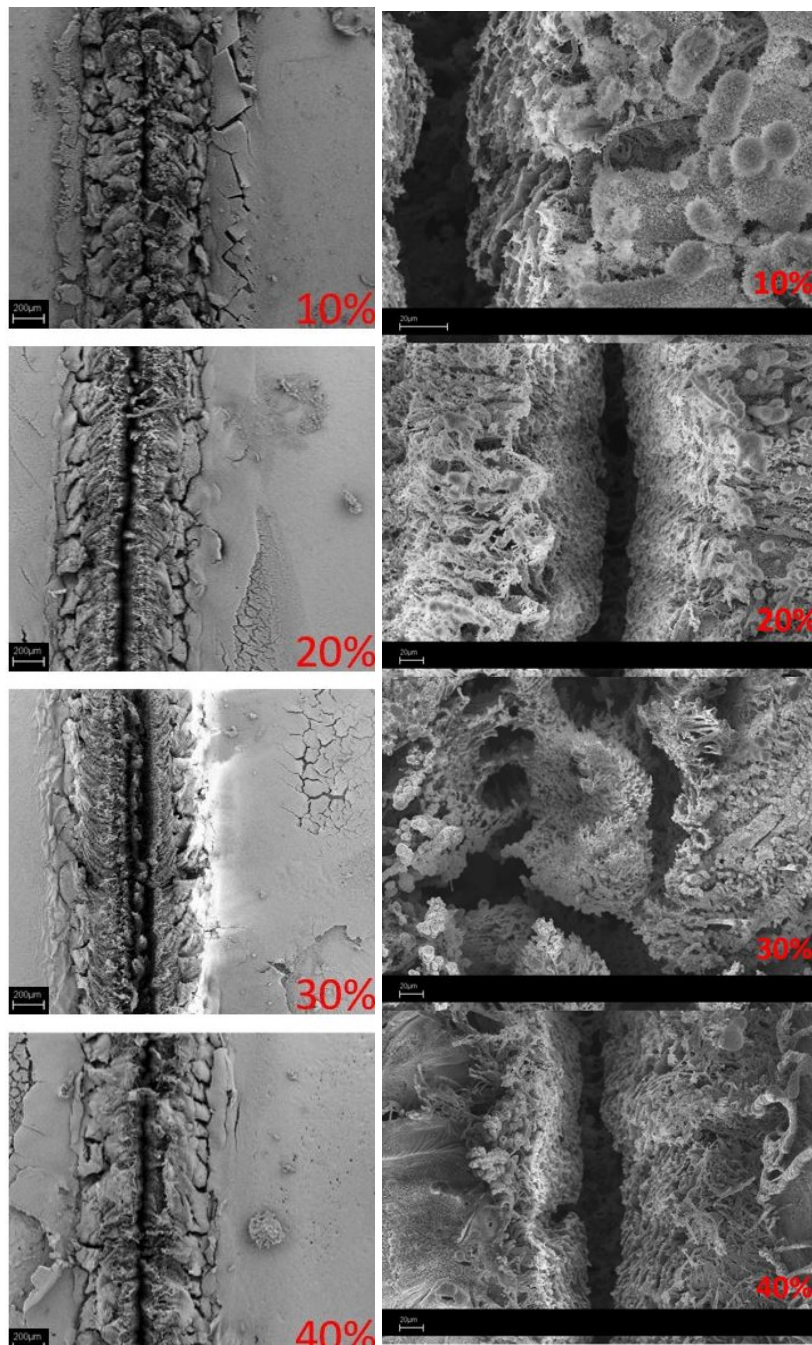


Figure 3.10: Comparison between Raman of LIG on PDMS and PDMS-TEG 40%

TEG from 10% to 40% in order to improve the investigation of the carbonized structure over the substrate.

The laser writing produce onto PDMS-TEG mixture a sort of porous structure, same phenomena of Ref. [9] but onto polyimide. From the pictures it is possible to notice a deep crevice at the beam center. The morphological changes increase raising the laser power that results more porous. This behaviour was already described in Ref. [9].

According to Ref. [9] the explosive phase change can lead to the hydrodynamic expulsion. This can cause the generation of microhills around the area of ablation. This behaviour is clear from picture 3.11.



(a) Fesem of PDMS-TEG mixture at a scale of 200 μm (b) Fesem of PDMS-TEG mixture at a scale of 20 μm

Figure 3.11: Fesem of PDMS-TEG mixture at a scale of 200 μm and 20 μm

3.3.3 Mechanical tests

In this section are present the results of the mechanical tests performed onto different substrates in order to find if there are huge differences between the pure PDMS and the ones that contain TEG in different percentage.

The aim is to find the Young's modules (E) of the substrates and compared to literature results about PMDS. It is defined as in equation 3.3.

$$(3.3) \quad E = \frac{\text{Stress}}{\text{ElasticStrain}} = \frac{Fl_0}{A\Delta l}$$

where F is the force applied in Newton, l_0 is the length of the substrate, A is the cross-sectional area, so is equal to the thickness multiplied by the wide, Δl is the difference between the length when the force is applied and the initial length l_0 .

To perform these measurements the machine used is Instron 2712-003, shown in fig.3.12. It can apply a maximum pressure of 6 Bar and a maximum load of 1 kN. The measurements are performed at a velocity of 5 mm each minute.

The substrates tested are more samples for PDMS, PDMS-TEG10%, PDMS-TEG20%,



Figure 3.12: Instron model 2712-003, machine use to perform mechanical tests

PDMS-TEG30%, PDMS-TEG40% substrates.

The Young's module obtained it is approximately the same for all these substrates. The values ranging between (0.66-0.76)MPa for PDMS-TEG40%, (0.67-0.91)MPa for PDMS-TEG30%, (0.75-0.86)MPa for PDMS-TEG20% and (0.91-1.13)MPa for PDMS-TEG10%.

This variation of Young's module is caused by the TEG present. Triethylene glycol, as already known from section 3.2.2, is a viscous liquid, more dense than water. It is obvious that adding it into PDMS improve the stretchability, in fact due the amount added each time the variation in the results are obtained.

However, in general, it is possible to notice that increasing the percentage of TEG into

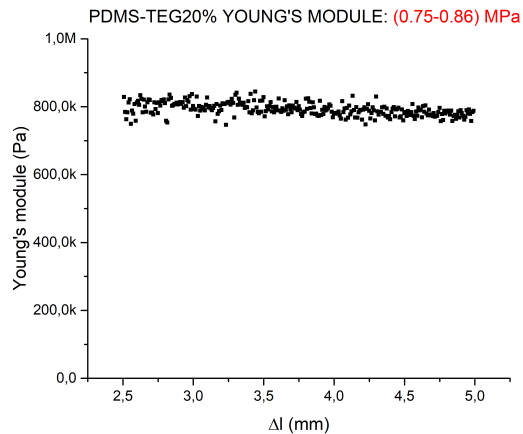


Figure 3.13: Young's module plot versus the deformation $\Delta l = l - l_0$

PDMS the Young's module decrease a little. As matter of fact the compared value for pure PDMS is (1.41-1.56)MPa. An example of plot of Young's module variation versus the ratio between $\Delta l/l$ is shown in fig. 3.13.

DEVICES FABRICATION AND CHARACTERIZATION

In this chapter the devices made and tested are presented. Thanks to characterization performed in chapter 3 the best writing parameters are evaluated and with these the devices are assembled.

In the first part the strain sensors created are analyzed and compared onto the different substrates. In the second part the supercapacitors made onto PDMS and TEG are inserted varying the percentage of TEG from 10 % to 40 % in weight.

Two important comparison are evaluated. The first is the one that compare PDMS and TEG in general. The second one is the one that compare the different percentage of TEG. Current/voltage characteristics were recorded with an inline two-point probe configuration using a Keithley 2635A source measure unit for evaluate strain gauges behaviour. Instead for electrochemical measurements on supercapacitors a potentiostat/galvanostat 'Metrohm Autolab PGSTAT128' and with the respective software 'Nova 2.1 are used'

4.1 Strain sensors

The strains presented in the following subsection are divided according to the different type of substrates in order to obtain a clearer final comparison between the devices. The best result is obtained with Kevlar-PDMS strains but on the other side there is a loss in flexibility. A trade-off must be find, so the PDMS-TEG strains result to be the best devices in order to respect characteristics.

Then some strain gauges have been realized on Aramide substrates and bending tests

have been performed.

The gauge factor (GF), that is a common figure to show the sensitivity of electrical shift to mechanical deformation [24], is evaluated.

Ref. [24] explains that the that perfect graphene has little resistance change under strain, in fact its gauge factor is around 2. However other research ([24]) found that the transferred graphene on PDMS grown by CVD has a higher gauge factor approximately near 151.

The state of the art graphene-based composites typically exhibit gauge factors in the range of 2 up to 50, as shown in Ref. [13].

4.1.1 LIG strain sensors on PDMS substrate

Following the laser writing parameters of section 3.2.1, two working strains are been studied, they are presented in fig. 4.1.

The values of R_S of this two devices are not very good. The R_S of strain2 is 154898 Ω/\square and the R_S of strain1 is 4440 Ω/\square and the parameters of writing are under the fig. 4.1. This devices are too fragile so there is not the possibility to perform bending tests. Due to these high values of R_S it is better to develop the study of strain made of PDMS-TEG presented in section 4.1.2.

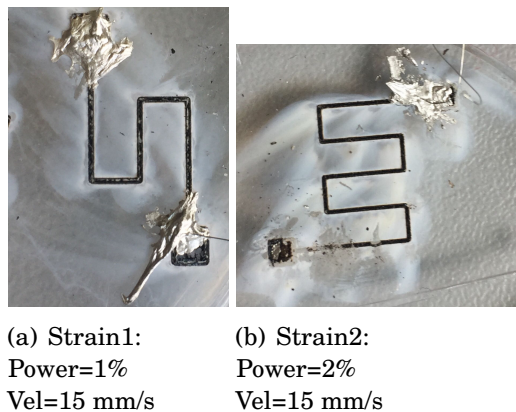


Figure 4.1: Strains made on pure PDMS substrates written at the same frequency of 15 kHz and 2 repetitions

The PDMS strain bending tests are not been performed because of the fragility of the material, the bend movements produce cracks into the material, loosing completely the conductivity.

Some measurement tests have been performed using PDMS to cover the devices in order

to avoid the cracks. However the obtained effect was the opposite, the strain sensor lost completely its conductivity. This may be is due to the fact that when the PDMS is poured over the strain, it starts to expand, but during this movements it takes away also some part of LIG materials.

4.1.2 LIG strain sensors on TEG substrates

According to the results obtained in section 3.2.2, strain are been written onto 8 different TEG-PDMS substrates, 2 types, one thicker (indicated with 'A') that the other (indicated with 'B'), for the 4 different percentage of TEG. The laser parameters used to write this strains are listed in table 4.1.

Table 4.1: Working parameters of laser writing of PDMS-TEG strain sensors

Substrates	Name	Geometry	Freq(kHz)	Power(%)	Vel(mm/s)	n° of Rep
10%A	a	Strain 22mm	10	5	5	2
10%B	b	Strain 22mm	10	5	10	2
40%A	c	Strain 22mm	10	5	10	2
40%B	d	Strain 22mm	10	5	7	2

The resulted values of R_S are plotted in fig.4.2.

A bending test was carried out and plot in fig. 4.3. The LIG patterns, written in zig-zag configuration has a length of 2.9 cm and is 0.1 cm wide. The laser writing parameters are 5 % of Power, 10 kHz of frequency, 5 mm/s of velocity and 2 repetitions.

For the bending test 4 different bending radius were used. To calculate the gauge factor, the equation 4.1.2 of Ref. [13] is used.

$$GF = \frac{(R - R_0)}{R_0} * \frac{2a}{h}$$

where $\frac{2a}{h}$ is ϵ , the bending induced tensile strain, a is bending radius and h the thickness of the sample.

Using this formula the gauge factor range between 8 to 11.

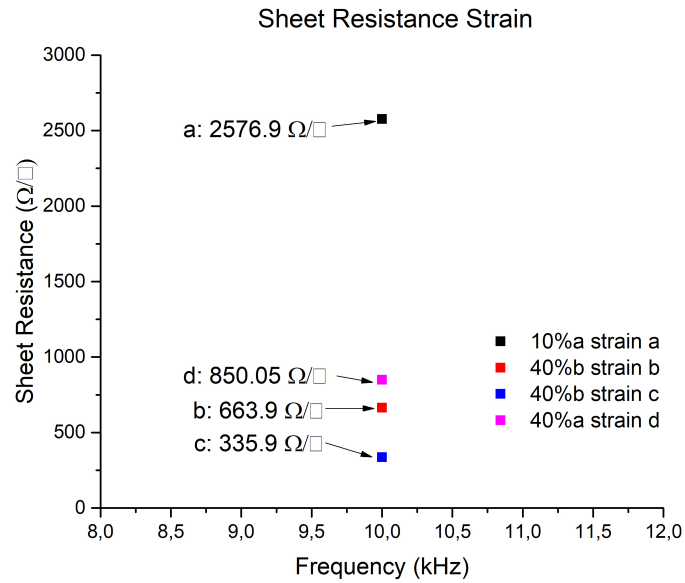


Figure 4.2: Value of R_S of PDMS-TEG strain for different substrates and parameters of laser writing

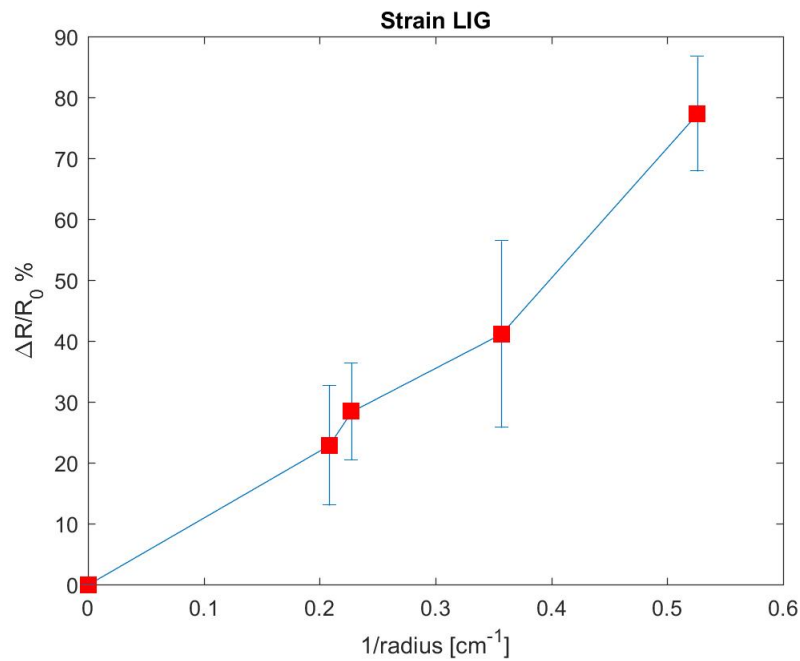


Figure 4.3: variation OF $\Delta R/R_0 \%$ testing the bending of the PDMS-TEG device with different bending radius

4.1.3 LIG Strain sensors on different substrates

As in section 3.2.3 this section is divided into two main parts. The first one deals with the LIG strains made onto Kevlar substrate and the second one with the materials that contain Aramide.

In the Kevlar substrate, described in section 3.2.3 two working strain are been analyzed. The laser parameters set of the two strains are same frequency, 10 kHz, same velocity, 5 mm/s, same number of repetitions, 2, but different power, in the first one was set to 10% and in the second one to 20%.

The results expressed in Sheet Resistance change a lot because the first strain has a $R_S = 924\Omega/\square$ and the second one has $R_S = 227.5\Omega/\square$. The reason why increasing the power there is an huge decrease in R_S is that the composite material made of Kevlar and PDMS contains the majority of the Kevlar fibers in the bulk of the substrate so increasing the power allows the laser beam to reach the inner part, richer of Kevlar fibers.

The bending test was not possible to be performed because the substrate obtained with this mixture lost its flexibility due to the Kevlar fibers.

In this second part of the section the working strain gauges made onto materials previous

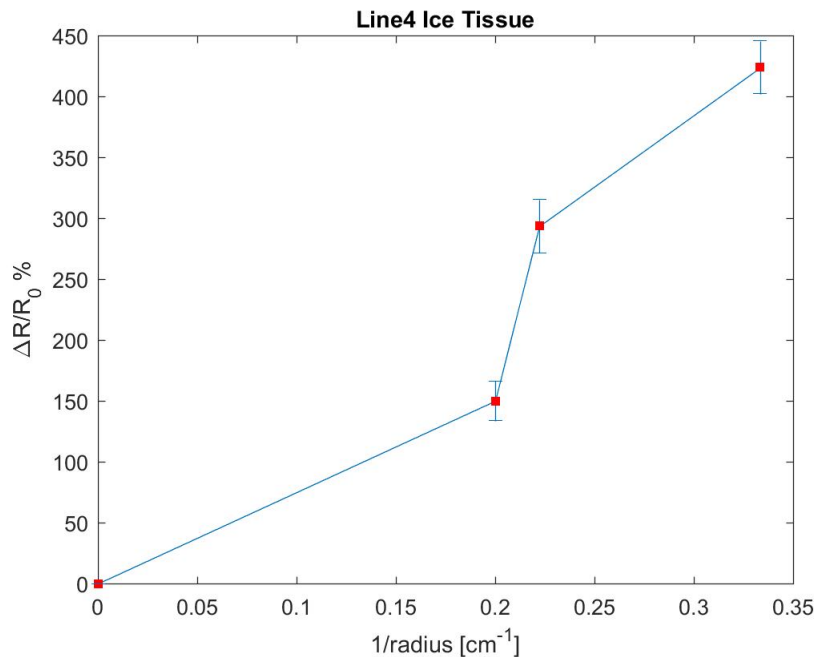


Figure 4.4: According to the bending of the device the $\Delta R/R_0\%$ there is a strong variation in $\Delta R/R_0\%$ in line4 of Ice substrate

characterized are tested. Also bending measurements onto conductive lines are possible because of the good adhesion of LIG material onto the samples.

Firstly, bending test of line1 of 'Orange tissue' and line4 of 'Ice tissue' are performed and the result variation are plot in fig. 4.4.

In the 'y axis' it is shown the ratio between ΔR and R_0 , where R_0 is the resistance in flat conditions without any bending movement performed, ΔR is the difference between R , resistance at a certain angle of bending, and R_0 . Instead in the 'x axis' $1/\text{radius}$ is plotted, expressed in cm^{-1} .

The plot of line 1 of 'Orange tissue' is not present because after the measurements the line cracks. However the fig.4.4 of line 4 of 'Ice tissue' is possible to notice that the device is extremely sensitive to bend because it reaches an increase of 450% respect to the flat position.

The slope of the $\Delta R/R_0\%$ vs $1/\text{radius}$ is not uniform, in fact from a radius of 4.8 cm to one of 4.4 cm the slope raises extremely fast coming back to the previous one until 2.8 cm of radius.

4.2 Supercapacitors

In this section the supercapacitors performance are evaluated from cyclic voltammetry measurements and constant current charge/discharge.

As in the previous section, this section is divided into 2 subsection according to the substrate type, the first one is the one with 'pure' PDMS and the second one is with TEG-PDMS.

In the last part of the section a comparison between the SCs made on the different substrate is carried out, in particular a comparison between the devices made on the different percentage of TEG inserted into PDMS is evaluated in order to find the optimum features.

Then a final comparison between the supercapacitors made onto PDMS and best one made onto PDMS-TEG.

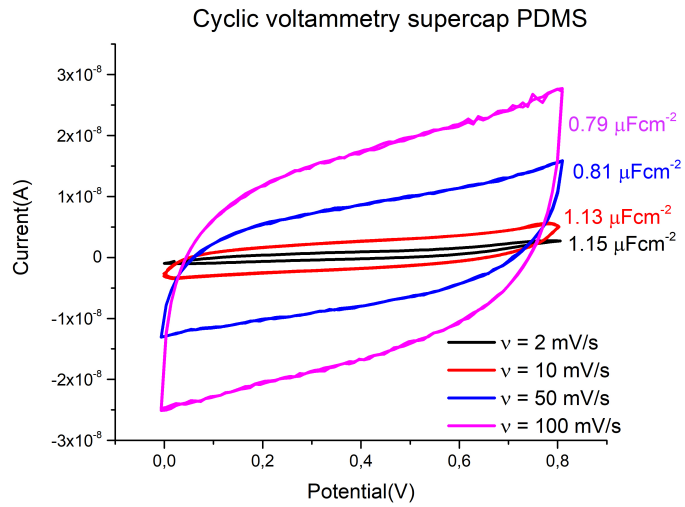
All the devices are analyzed using the same aqueous electrolytes 1M Na_2SO_4 .

All measurements were acquired with a potentiostat/galvanostat 'Metrohm Autolab PGSTAT128' and with the respective software 'Nova 2.1'.

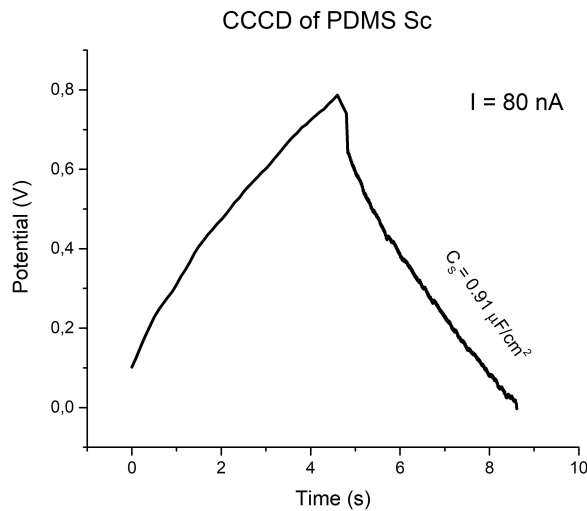
4.2.1 LIG supercapacitor on PDMS substrate

In fig.4.5 the electrochemical measurements performed on a supercapacitor made with LIG on PDMS written with the following parameters:

10 kHz of frequency, 3 % of power, 20 mm/s of velocity and 2 repetitions. It is resulted the best device written onto pure PDMS.



(a) Cyclic Voltammetry at 4 scan rate of PDMS Sc



(b) CCCD of Sc

Figure 4.5: Electrochemical measurements of PDMS supercapacitor

As shown in fig.4.5a, considering an area of 0.414cm^2 , the bigger specific capacitance is $1.58\mu\text{F}/\text{cm}^{-2}$ at a scan rate of 50 mV/s .

This value is too low compared to the one of supercapacitors made onto polyimide (Ref.[1]), shown in fig.4.6 that reaches a C_S of $201\mu\text{F}/\text{cm}^{-2}$.

Instead the plot of fig.4.5b shows a constant current charge/discharge only with a current of 80 nA because other changes in current rate are not been possible because,

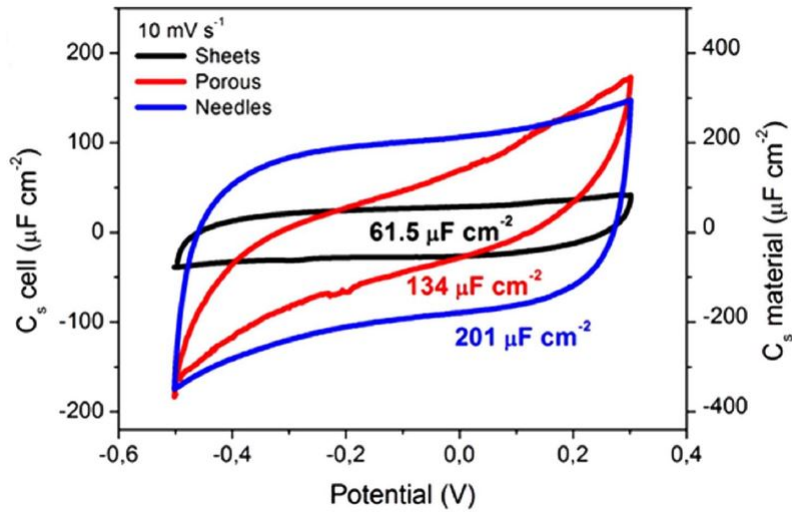


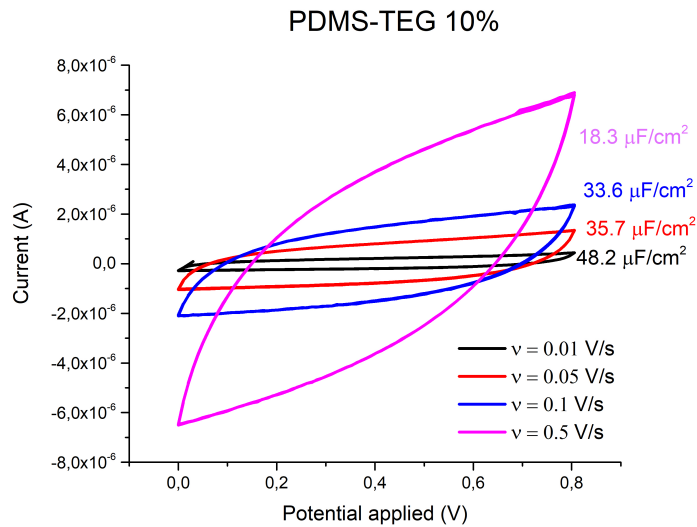
Figure 4.6: Cyclic voltammetry at 10 mV/s of a supercapacitor made onto polyimide [1]

unfortunately, the contacts have detached during the measurements.

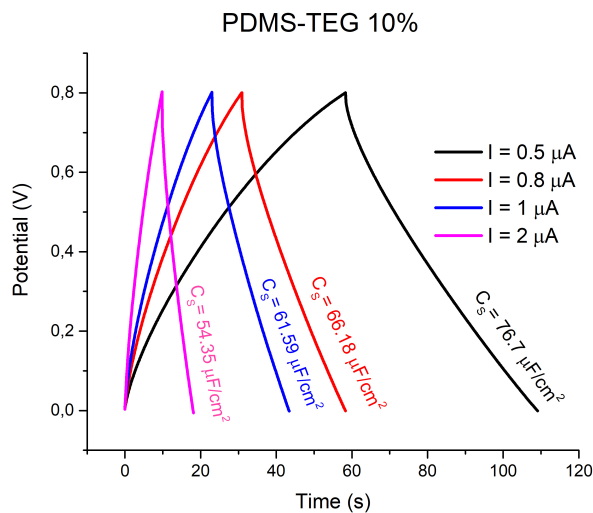
However The rectangular shape of the cyclic voltammetry and the triangular one of the CCD imply a good behaviour of electrical double layer that it is surely influenced by the low conductivity of PDMS.

4.2.2 LIG supercapacitor on TEG substrates

In this subsection the CV and constant current charge/discharge are inserted, plotted according to the percentage of TEG present into PDMS. All these supercapacitors are written with the same laser parameters that are: 10 kHz of frequency, 5 % of power, 5 mm/s of velocity, 2 repetitions in ambient atmosphere conditions in order to evaluate a coherent comparison.



(a) Cyclic Voltammetry at 4 scan rate of PDMS-TEG 10% Sc



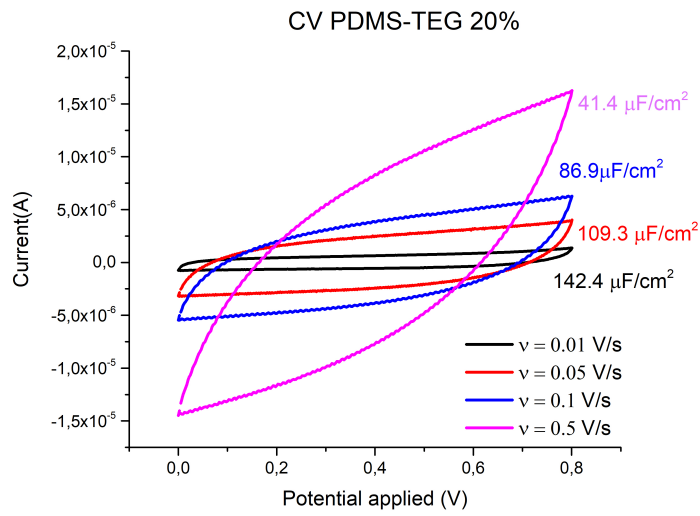
(b) CCCD of PDMS-TEG 10% Sc

Figure 4.7: Electrochemical measurements of PDMS-TEG 10% supercapacitor

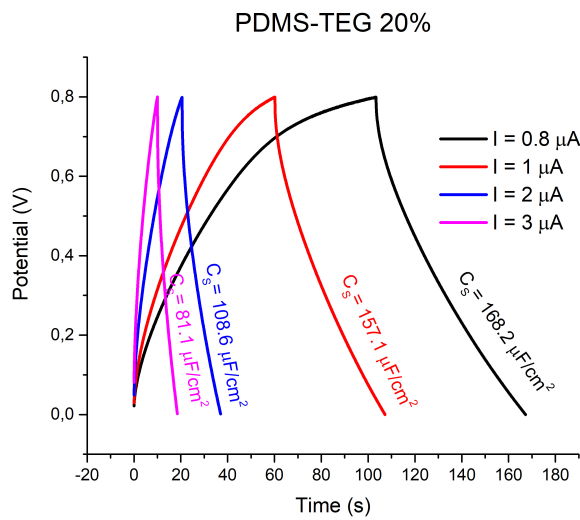
The first one plotted is in fig.4.7. The specific capacitance reaches $46.2\mu F/cm^2$, ten times more respect the supercapacitor made onto pure PDMS.

Thanks to the fig.4.7b it is possible to compare the values of specific capacitance obtained by the constant current charge/discharge, the maximum value reached is $76.7\mu F/cm^2$ with a current of $0.5\mu A$.

The fig.4.8 represents the plot of the CV and CCCD of the SC made onto PDMS-TEG 20%. It must be highlighted the specific capacitance at 10 mV/s that is equal to $142.4\mu F/cm^2$, that is a value that results triple compared to PDMS-TEG 10%. (fig.4.7). In fig.4.8b the CCCD is plotted changing the current between three values 1,2 and $5\mu A$. Choosing the same rate of current, $2\mu A$, in fig.4.7b and fig.4.8b, the value of specific capacitance is approximately doubled from $76.7\mu F/cm^2$ to $156.39\mu F/cm^2$. A big improvement.



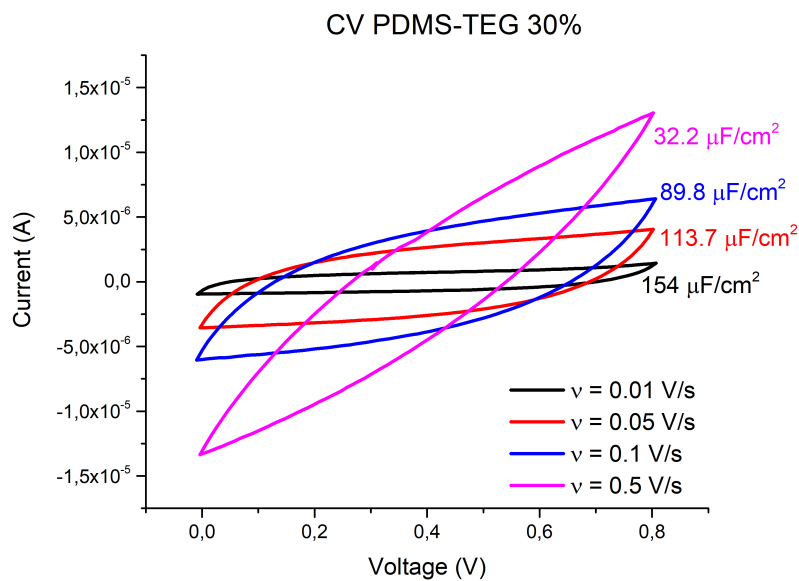
(a) Cyclic Voltammetry at 4 scan rate of PDMS-TEG 20% Sc



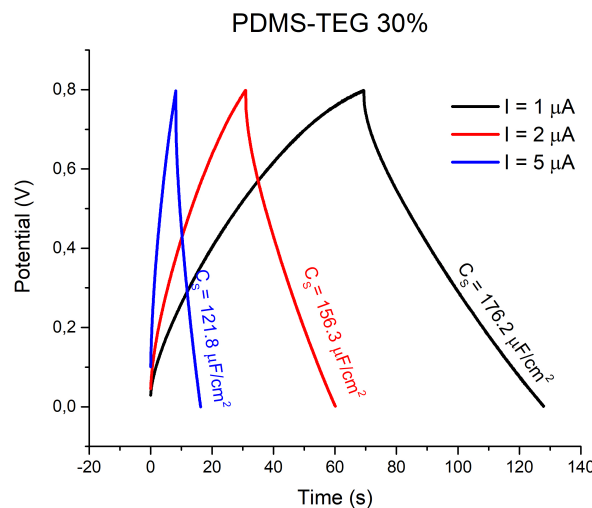
(b) CCCD of PDMS-TEG 20% Sc

Figure 4.8: Electrochemical measurements of PDMS-TEG 20% supercapacitor

The CV of PDMS-TEG 30% is shown in fig.4.9. Compared to the others CV, there 4 different scan rate are plotted. The bigger specific capacitance results with the lowest scan rate, 10 mV/s, and it is equal to $154 \mu\text{F}/\text{cm}^2$. Respect to the value of fig.4.6 at the same scan rate 10 mV/s the value is still lower, because it is $154 \mu\text{F}/\text{cm}^2$ compared to the $201/\text{cm}^{-2}$ of polyimide Sc.



(a) Cyclic Voltammetry at 4 scan rate of PDMS-TEG 30% Sc

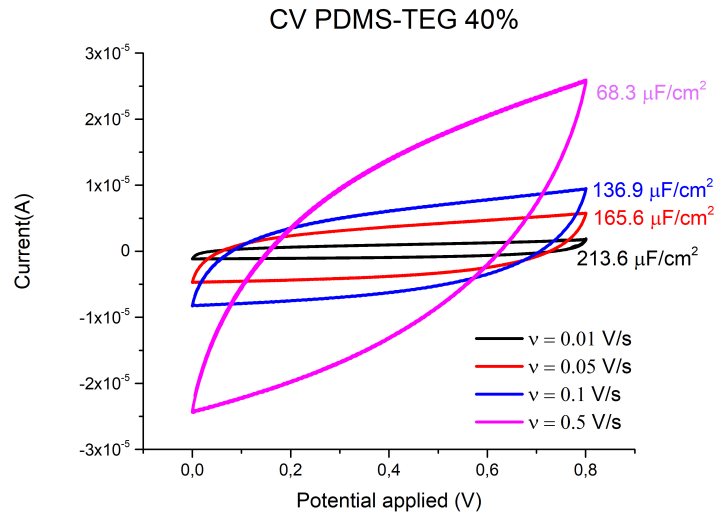


(b) CCD of PDMS-TEG 30% Sc

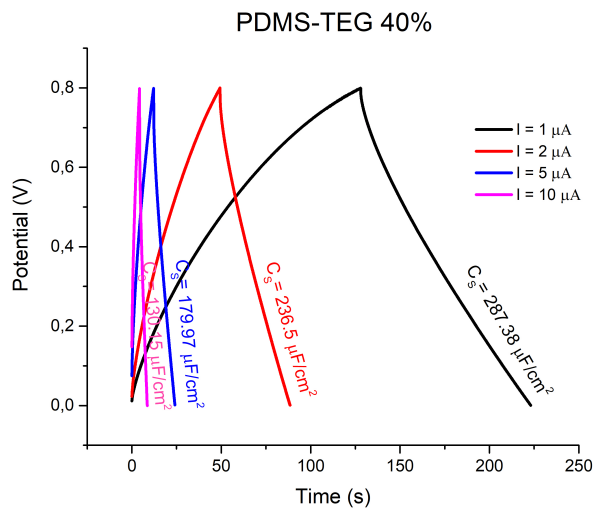
Figure 4.9: Electrochemical measurements of PDMS-TEG 30% supercapacitor

In fig.4.10 extremely good results are reached compare to the initial pure PDMS, with a scan rate of 10 mV/s, the specific capacitance result $213.6 \mu F/cm^2$.

This result, not only is 200 times bigger compared to the CV of PDMS Sc, but it also doubled compared to the one of Ref.[1] of fig.4.6.



(a) Cyclic Voltammetry at 4 scan rate of PDMS-TEG 40% Sc



(b) CCCD of PDMS-TEG 40% Sc

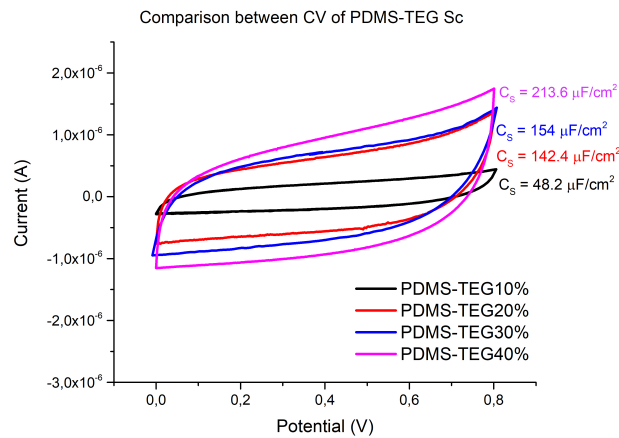
Figure 4.10: Electrochemical measurements of PDMS-TEG 40% supercapacitor

Also with CCCD of PDMS-TEG 40% important improvements are obtained, with the same value of current of $2 \mu A$ of fig.4.7b the resulted value of C_S is $76.7 \mu F/cm^2$ instead

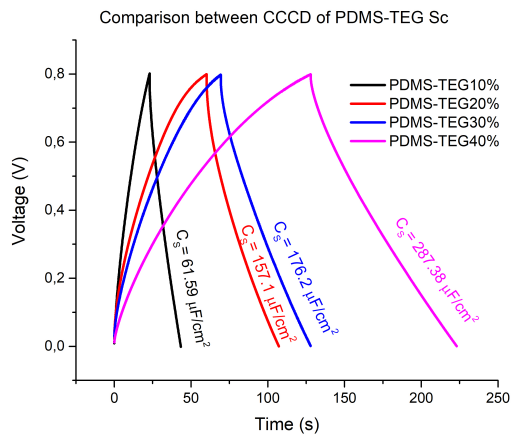
in fig.4.10b the value is $236.5\mu F/cm^2$.

4.2.3 Comparison between LIG supercapacitor on different percentage of TEG into PDMS substrate

In this subsection a comparison between the cyclic voltammetry 4.11a of PDMS-TEG at 10 %, 20 %, 30 %, 40 % is carried out. The scan rate used to plot is 10 mV/s. From the graph it is evident that the shapes of the these CV tend to reach the ideal rectangular shape. All these supercapacitors are written using the same laser parameters (10kHz of frequency, 5 % of power, 5 mm/s of velocity and 2 repetitions).



(a) Comparison between CV of PDMS-TEG Sc, varying the % at a scan rate of 50 mV/s



(b) Comparison between CCD of PDMS-TEG Sc, varying the %

Figure 4.11: Electrochemical measurements, CV (at 50 mV/s) and CCD ($I = 1 \mu\text{A}$), of PDMS-TEG Sc, varying the % in weight of TEG

According to the predictions given by section 3.2.2 the behaviour of these devices are correct and the best result is the one made on PDMS-TEG 40 %.

Increasing the percentage of TEG into PDMS the resulted specific capacitance at 10 mV/s of scan rate increase. Starting from $48.2 \mu\text{F}/\text{cm}^2$ at 10 %, then $142.4 \mu\text{F}/\text{cm}^2$ at 20 %, $154 \mu\text{F}/\text{cm}^2$ at 30 % and $213.6 \mu\text{F}/\text{cm}^2$ at 40 %.

From fig.4.11a it is evident that the shape of CV of PDMS-TEG at 20% tends to be near to the one of 30% but the area divided by two times the voltage window multiplied by the scan rate and the total divided by the Sc area, that represents the specific capacitance, results a little above 10%, as expected from section 3.2.2.

In the table 4.2 there are resumed the results of the specific capacitance obtained from the different percentage of TEG.

Table 4.2: Summary of the C_S results obtained from the Cv of different percentage of TEG into PDMS

Scan rate	10%	20%	30%	40%
0.01 V/s	$48.2 \mu\text{F}/\text{cm}^2$	$142.4 \mu\text{F}/\text{cm}^2$	$154 \mu\text{F}/\text{cm}^2$	$213.6 \mu\text{F}/\text{cm}^2$
0.05 V/s	$35.7 \mu\text{F}/\text{cm}^2$	$109.3 \mu\text{F}/\text{cm}^2$	$113.7 \mu\text{F}/\text{cm}^2$	$165.6 \mu\text{F}/\text{cm}^2$
0.1 V/s	$33.6 \mu\text{F}/\text{cm}^2$	$86.9 \mu\text{F}/\text{cm}^2$	$89.8 \mu\text{F}/\text{cm}^2$	$136.9 \mu\text{F}/\text{cm}^2$
0.5 V/s	$18.3 \mu\text{F}/\text{cm}^2$	$41.4 \mu\text{F}/\text{cm}^2$	$32.9 \mu\text{F}/\text{cm}^2$	$68.3 \mu\text{F}/\text{cm}^2$

4.2.4 Comparison between LIG supercapacitor on PDMS and PDMS-TEG substrates

In this section a conclusive comparison between the devices onto pure PDMS and the best mixture of PDMS-TEG is evaluated.

Before between the cyclic voltammetry (fig. 4.12 and then between the constant current charge/discharge (fig. 4.13).

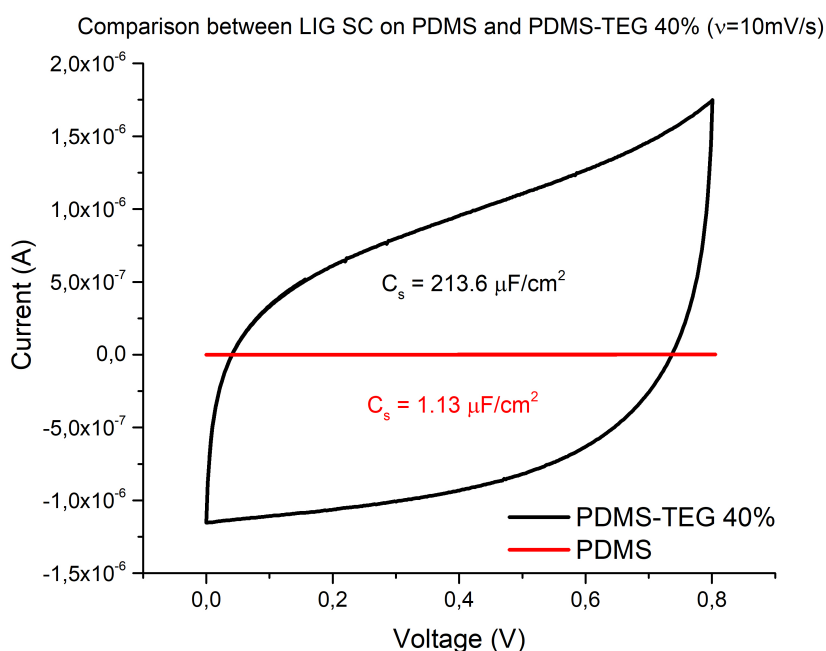


Figure 4.12: Comparison between cyclic voltammetry at 10 mV/s of LIG SC on PDMS (red) and PDMS-TEG 40% (black)

Starting from the point reached in section 4.2.3, that evaluates as the best PDMS-TEG device the one with a percentage of TEG of 40% into PDMS, the conclusions are herein resumed.

It is evident that the specific capacitance of PDMS-TEG 40% (Fig. 4.12 black line) is approximately 200 times bigger than the one made onto PDMS substrate (Fig. 4.12 red line), also the current that the PDMS device reaches is $75 \text{ nA}/\text{cm}^2$ versus the one of fig.?? that is $75000 \text{ nA}/\text{cm}^2$. A really huge amount of current more obtained.

The same considerations done for the cyclic voltammetry are clear also from the constant current charge/discharge of Fig. 4.13. There an enormous difference between the specific capacitance evaluated and the amount of constant current applied is

completely different during the same time.

It is possible to notice that the IR drop quite visible in chart 4.13 black line, instead in picture 4.13red line is not so evident.

In fact the specific capacitance obtained by the constant current charge/discharge of LIG SC on PDMS-TEG 40% is $130.15 \mu\text{F}/\text{cm}^2$ compared to the one of pure PDMS equals to $0.91 \mu\text{F}/\text{cm}^2$ applying a current of 80 nA.

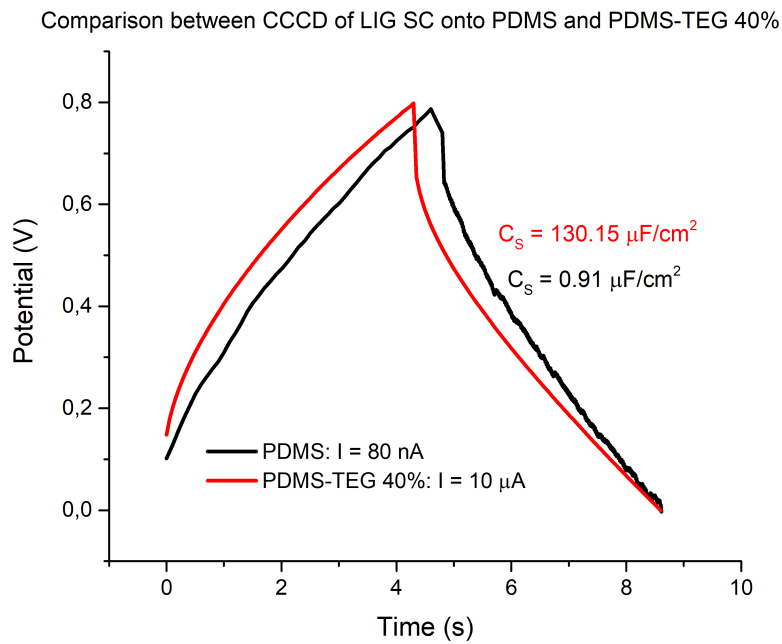


Figure 4.13: Constant Current charge/discharge of PDMS and PDMS-TEG supercapacitors

CONCLUSION

In this chapter the conclusion of this work are discussed.

The conclusion chapter is divided into two parts. The first described the main results obtained, focusing on the devices characterized, in particular on the supercapacitors. The second part deals with some possible improvements regarding the devices, in particular it describes other geometries that can be tested, other type of electrolytes that can be used.

5.1 Main results

It is necessary to start from the first initial aim of this work: verify if PDMS is an available substrate to obtain laser induced graphene.

This point is surely reached. The second purpose was to create a working energy storage device onto PDMS substrate. As shown in fig. 5.1 the second step is obtain. The third target was to find some improvements for the devices onto pure PDMS. The problem was related to the graphitization of the material. The amount of material converted into LIG was to low. The starting point was to find the optimum parameters of writing.

After these PEDOT:PSS coating was tested after plasma treatment of PDMS in order to increase the conductivity but the results was not so extraordinary, so other ways were chosen [19].

The idea to add other substances in order to increase the carbon content to PDMS was good. The materials tested were a lot: polyethylene glycol (PEG) addition, ascorbic acid

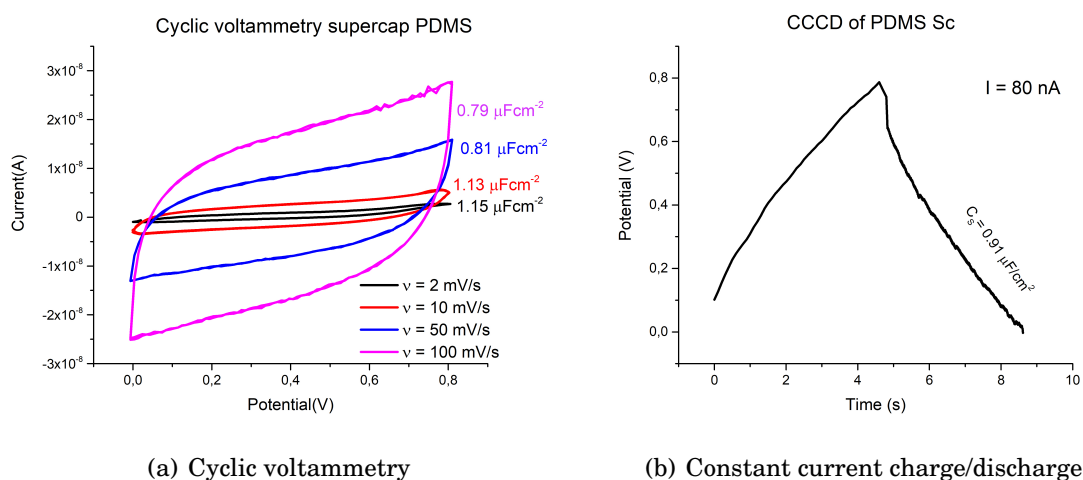


Figure 5.1: Supercapacitor made onto pure PDMS substrate with laser induced graphene

addition (commonly known as C Vitamin), Carbon fibers addition, Kevlar fibers addition, Boron (B) addition and triethylene glycol (TEG) addition .

These compounds were chosen because of their chemical structures, their easy market available, their low cost, their possibility of be inserted into PDMS without difficult processes, except for Boron.

Analyzed the LIG patterns obtained the best results was with the addition of TEG. This primitive mixture of PDMS and TEG (25% in weight) improved of a quite big amount the supercapacitors performances. Thanks to this a study according the variation due to the percentage of TEG in weight into PDMS was carried out. As shown in this master thesis the quantities chosen was 10%, 20%, 30%, 40% in weight. No more percentage of TEG was possible to insert into PDMS because TEG no more dilute into PDMS with these huge amounts.

In order to justify and completely characterize this way taken, the mixture PDMS-TEG was studied under different point of view:

- Conductivity of LIG patterns;
- Raman spectroscopy;
- Scanning electron microscopy;
- Mechanical test with evaluation of Young's module;
- Performance of LIG supercapacitors;

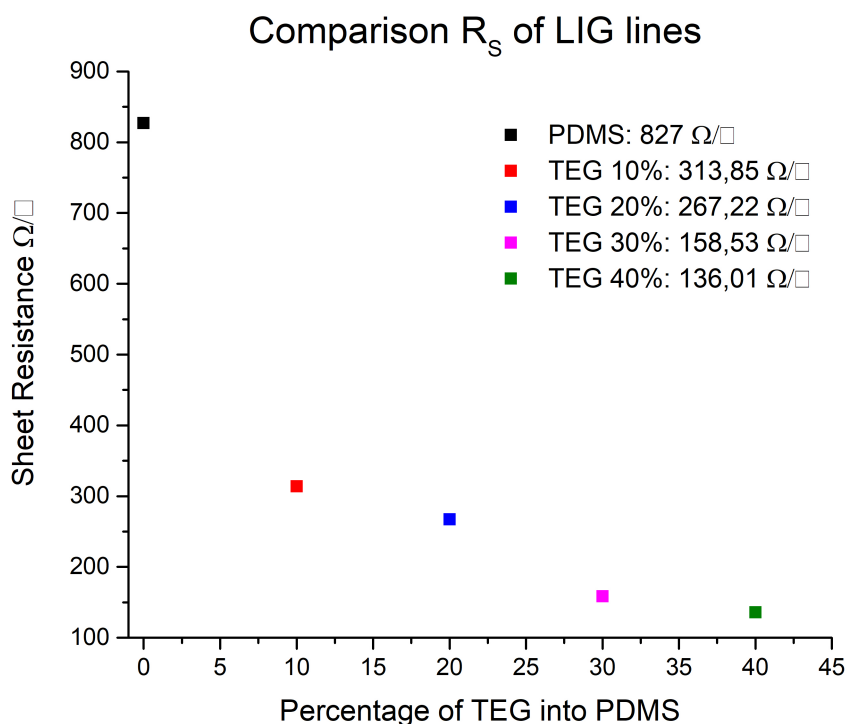


Figure 5.2: Sheet Resistance variation increasing the percentage of TEG into PDMS

- Performance of LIG strain gauge;

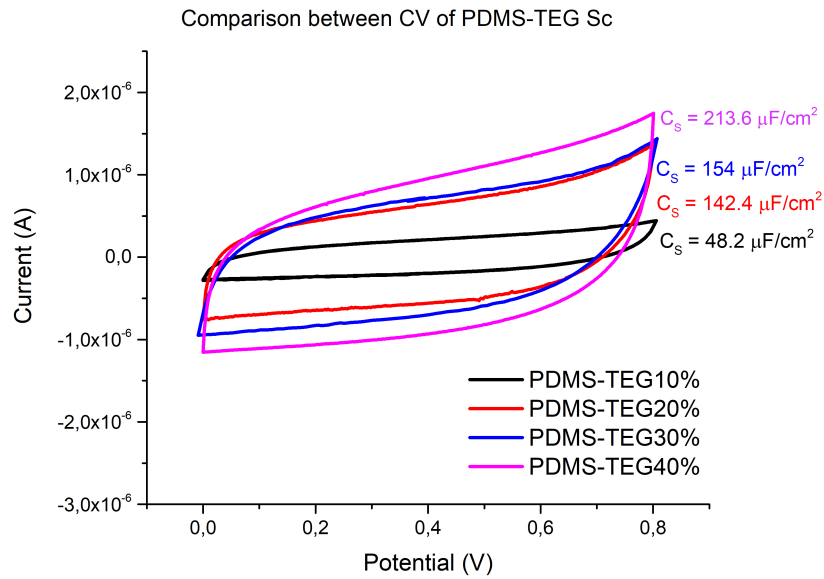
All tests listed before have been carried out for all the samples: PDMS and PDMS-TEG mixture in different %. The aim was to find a specific trend and to analyzed the results in order to make, also, comparison with literature.

According to the first point of the list, the conductivity of LIG lines onto PDMS-TEG was tested and a specific trend was found. The plot is in fig. 5.2. It possible to notice the trend, increasing the percentage of TEG into PDMS, there an improvements in the performances of the devices.

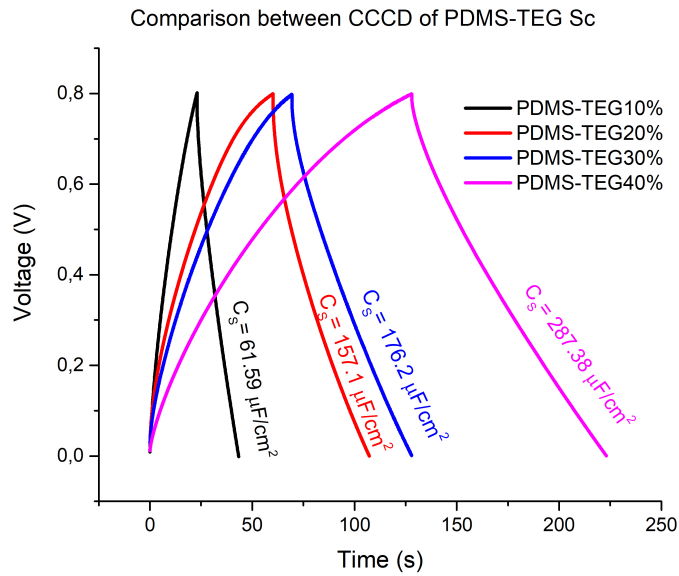
With PDMS-TEG 40% the value of R_S goes down to $136.01\Omega/\square$. Thanks to the good results obtained during the conductivity tests, also the performances of PDMS-TEG supercapacitors are evaluated.

The Cyclic voltammetry and CCD obtained are shown in fig. 5.3, plot on the same chart in order to find the differences.

It's clear from Fig. 5.3 that the values of specific capacitance grow up proportionally to the amount of TEG present. This trend is justify from the plot of fig. 5.2.



(a) CV of PDMS-TEG for different percentage



(b) CCCD of PDMS-TEG for different percentage

Figure 5.3: Comparison between the CV and CCCD of LIG SC for different percentage of TEG into PDMS

The results obtained of pure PDMS Scs and PDMS-TEG 40% are deeply described in section 4.2.4.

In summary the value of C_s with a scan rate of 10 mV/s is equal to $1.13 \mu\text{F}/\text{cm}^2$ for

PDMS Scs, to $201 \mu F/cm^2$ for the best Sc of Ref. [1] and to $205 \mu F/cm^2$ for the PDMS-TEG 40% Sc. A huge improvements compared to the first PDMS SC.

The next step was to analyzed the differences in the LIG patterns made onto PDMS and PDMS-TEG mixture. To achieve this task Raman spectroscopy, Scanning electron microscopy and X-Ray photoelectron spectroscopy were used.

Starting from the Raman spectroscopy the plot obtained are shown in Fig. 5.4, more details are in section 3.3.

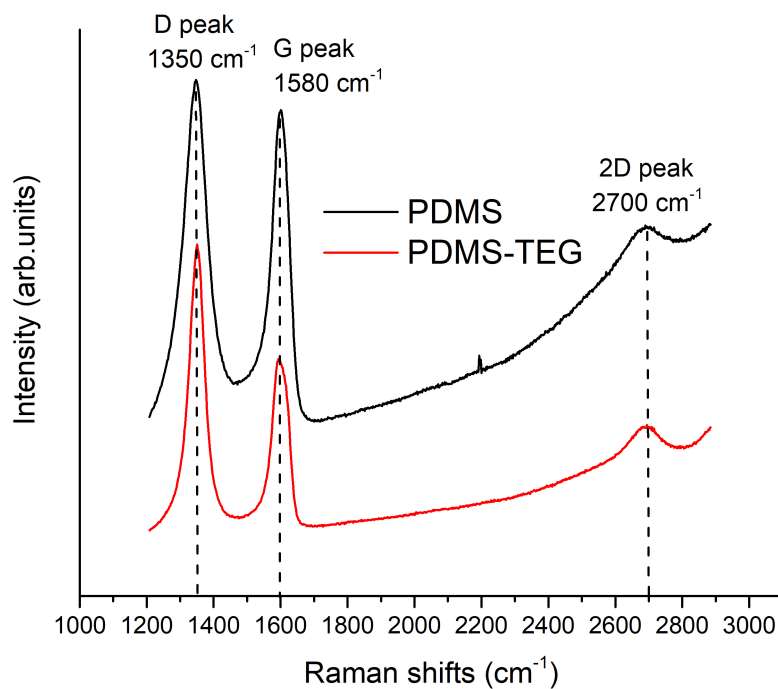


Figure 5.4: Comparison of Raman spectroscopy

To summarize, from fig. 5.4 are clearly seen the common peaks present in a Raman spectroscopy of graphene. The D peak at 1350 cm^{-1} , the G peak at 1580 cm^{-1} and a small second order 2D peak at 2700 cm^{-1} are shown.

The images acquired by means of Scanning electron microscopy (SEM) are visible in details in section 3.3 but, in conclusion, it is possible to say that from the images a trend increasing the percentage of TEG into PDMS is clear. There is a deep crevice at the beam center. The morphological changes increase raising the laser power that results more porous. As already foresight by Ref. [9] the explosive phase change can lead to the hydrodynamic expulsion. This can cause the generation of microhills around the area of

ablation. This behaviour is clear from picture 5.5, that represents the morphology of a line written onto PDMS-TEG 40%.

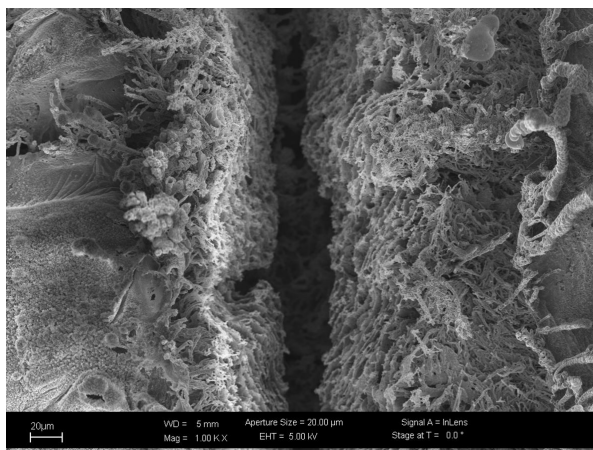


Figure 5.5: Scanning electron microscopy (SEM) of PDMS-TEG 40% line. There is a zoom onto the deep crevice located at the beam center.

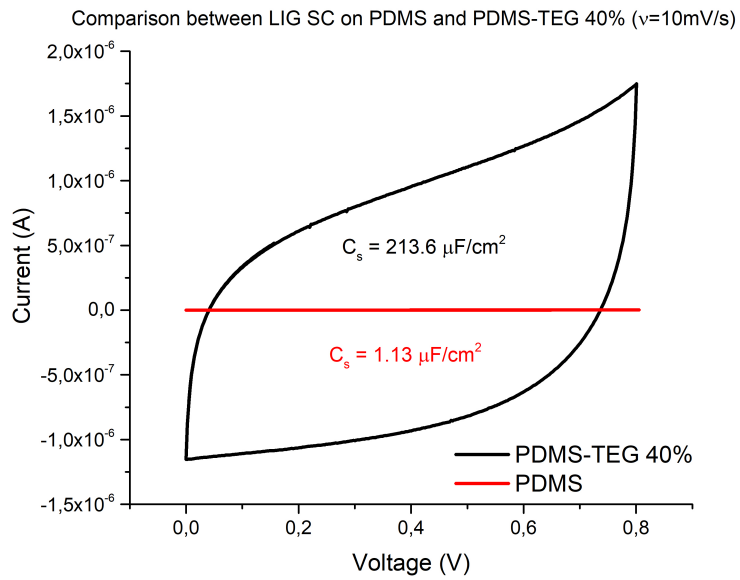
In order to complete the analysis about PDMS-TEG materials, mechanical tests (Section 3.3.3) were carried out. The purpose of these experiments is to find the difference of samples made of pure PDMS, PDMS-TEG in different percentages.

The final results of the analysis is to obtain the Young's modules of the compounds. The Young's module obtained it is approximately the same for all these substrates. The values ranging between (0.66-0.76)MPa for PDMS-TEG40%, (0.67-0.91)MPa for PDMS-TEG30%, (0.75-0.86)MPa for PDMS-TEG20% and (0.91-1.13)MPa for PDMS-TEG10%.

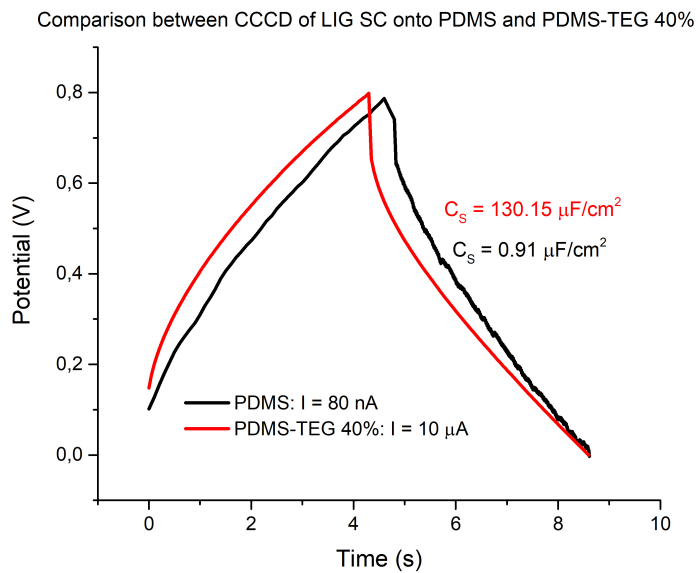
This little variation of Young's module is caused by the TEG presence, in fact TEG, as known from section 3.2.2, is a viscous liquid so its addition into PDMS improve the stretchability, so due the amount added each time the variation in the results are shown. A final comparison between the initial results of CV and CCCD of LIG supercapacitors made onto 'pure' PDMS and PDMS-TEG 40% are plot in fig. 5.6. It is clear from fig. 5.6a that the specific capacity obtained by the CV of LIG SC on PDMS-TEG 40% is quite 200 times that the one of pure PDMS.

From fig. 5.6b it is shown that in the same period of time the specific capacitance obtained by the constant current charge/discharge of LIG SC on PDMS-TEG 40% is $130.15 \mu F/cm^2$ compared to the one of pure PDMS equals to $0.91 \mu F/cm^2$ applying a current of 80 nA.

In order to find a performance comparison between the devices the Ragone plot are shown. In these charts in the 'y axis' there is the specific energy, expressed in Wh/cm^2 ,



(a) CV of LIG SC onto PDMS and PDMS-TEG 40%



(b) CV of LIG SC onto PDMS and PDMS-TEG 40%

Figure 5.6: Comparison between CV and CCCD of LIG supercapacitors made onto 'pure' PDMS and PDMS-TEG 40%

instead in the 'x axis' there is the specific power W/cm^2 . This plot is useful to compare any energy-storage devices [20]. The x axis shows how quickly the energy available, of 'y axis' can be delivered. As consequence the curves obtained are usually straight lines with a final slope. The specific Energy (E_S) and the specific power (P_S) are evaluated from eq. 5.1.

$$(5.1) \quad \begin{aligned} E_S &= \frac{V \times I \times t}{A} \\ P_S &= \frac{V \times I}{A} \end{aligned}$$

where V is the voltage applied, I the current, t the time and A the area expressed in cm^2 . To evaluate the Ragone's plot the cyclic voltammetry charts of section 4.2.2 and 4.2.1 are used, so 4 points are present because they indicate the 4 different scan rate. From fig.

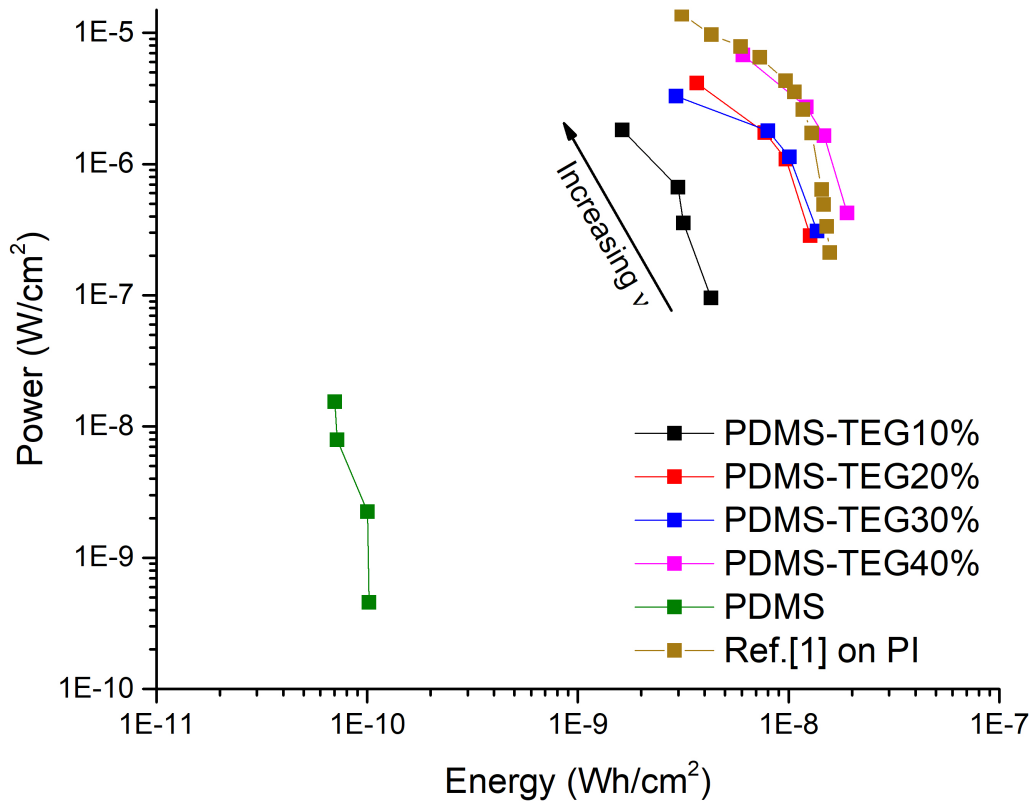


Figure 5.7: Ragone's plots of PDMS, PDMS-TEG 10%, PDMS-TEG 20%, PDMS-TEG 30%, PDMS-TEG 40% and Ref. [1] Supercapacitors

5.7 it is possible to see that good values of Power vs Energy are reached for PDMS-TEG

40% substrates. The values of PDMS supercapacitor are below of the ones of PDMS-TEG of a quite big amount. Instead the values of PDMS-TEG substrates are located more or less on the same area.

The Ragone chart of Ref.[1] is shown in brown in order to compare the results onto polyimide (PI) substrates with the ones of PDMS-TEG substrates.

To show in a better way the plot, a zoom of fig. 5.7 are in fig. 5.8.

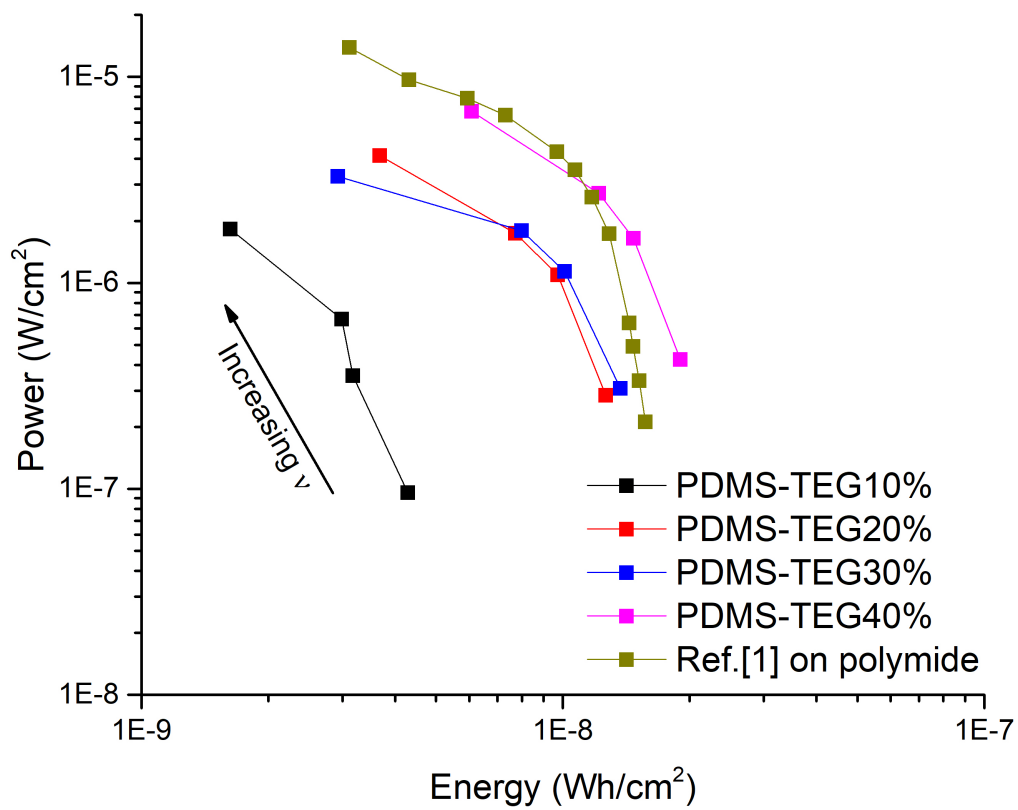


Figure 5.8: Ragone's plots of PDMS-TEG 10%, PDMS-TEG 20%, PDMS-TEG 30%, PDMS-TEG 40% and Ref. [1] Supercapacitors

From the Ragone's chart of fig. 5.8 it is possible to see that the values of power vs energy increases raising the percentage of TEG into PDMS. There are a value of percentage 30% that is located below one 20%, this value is derived from the two CV at a scan rate of 0.5 V/s (Section 4.2.2). However for the others results the trend is correct and inline with the one expected.

The Ragone's plot of the best result for Ref. [1] is plot in brown and is situated near the PDMS-TEG 40% Sc. The two plot are quite similar, however, for small scan rate the PDMS-TEG 40% Sc result the best one, although is made onto PDMS-TEG.

Thanks to a textile factory from Biella, that has provided different tissues made with Aramide some LIG patterns and strain gauges were made also onto different substrate, described in section 3.2.3 and section 4.1.3.

In general it is verified that is possible to build LIG strain sensors onto PDMS substrate. The main challenge to overcome is regarding the fragility of the devices. As verified in section 4.1.2 the bending tests onto PDMS strain gauges was not possible because when the LIG patterns are cover with PDMS, it infiltrates inside the structure damaging permanently the devices. However onto PDMS-TEG samples a working LIG strain gauges was analyzed. It is able to bend without cracking reaching a value of $\Delta R/R_0\%$ of 80 maintaining during the radius variation almost the same slope.

5.2 Possible improvements

In conclusion, regarding SCs, it is possible to state that all the initial targets of this master thesis are reached with results above the expectations.

The PDMS-TEG 40% has a Ragone's plot that is very similar to supercapacitor made onto polyimide. Compared the initial value of power, energy and capacitance for pure PDMS and for PDMS-TEG, the results obtained are quite good.

Obviously more studies in this direction should be carried out. In particular I think that a deep detailed studies onto the type of electrolytes that can be enhance over this one obtained can be tried. The one used in this work is 1M Na_2SO_4 , as in the previous chapter mentioned. The choice of this one was dictated by the fact that it is easy to find, it is cheap, it hasn't problem related to health security. However to improve the performances of the devices ionic liquid or polymeric gels can be tested. The first ones increase the voltage window and the thermal stability, instead the polymeric gels are easy to fabricate and they reduce the problems regarding the fast evaporation.

Another improvements and studies that can be analyzed are related to the device geometries. For example, concerning the interdigitated supercapacitors, the number of fingers was maintained fix in order to make comparison with sense. Although a variation in the number of fingers can be tested and simulated in order to find the optimum shapes.

Another improvement could be cover the LIG patterns with manganese dioxide (MnO_2) [10] by electrodeposition because it shows greatly improved electrochemical performance. Another type of pseudocapacitive material tested in Ref.[10] is ferric oxyhydroxide ($FeOOH$) representing characteristic transition metal oxides and conductive polymers. The same stream of consciousness can be followed for the contact geometries. In particular the type of wire chosen and the silver paint used. I used, as mentioned before, a preponderantly a bi-component silver paint provided by 'RS components S.r.l.' but the use of carbonius paint or mono-component paint should enhance the efficiency of the contact.

Instead, concerning the strain sensors a possible improvement that can be tested in order to overcome the adhesion problems of LIG materials is to cover the structure with a material that does not infiltrate into the device, such as PDMS or some enamel, but to use for example Kapton scotch that enable the conductivity and, at the same time, maintain the device compact and attached to the substrate.

BIBLIOGRAPHY

- [1] M. C. M. S. M. F. S. B. S. F. A. LAMBERTI, F. PERRUCCI AND E. TRESSO, *New insights on laser-induced graphene electrodes for flexible supercapacitors: tunable morphology and physical properties*, Nanotechnology, IOP publishing, (2017).
- [2] A. S. N. P. K. O. I. D. L. J. T. D. D. ANDRAS LAKI, ISMAEL RATTALINO AND P. CIVERA, *An integrated and mixed technology loc hydrodynamic focuser for cell counting application*, IEEE SENSOR, (2010).
- [3] F. I. ANINDYA NAG, SUBHAS CHANDRA MUKHOPADHYAY AND J. KOSEL, *Wearable flexible sensors: a review*, IEEE SENSOR, 17 (2017).
- [4] A. S. ANIS ALLAGUI, TODD J.FREEBORN AND B. J.MAUNDY, *Reevaluation of performance of electric double-layer capacitors from constant-current charge / discharge and cyclic voltammetry*, Scientif Reports, (2016).
- [5] H. J. N. CHARLES E. BAUER, *Iot wearable electronics revolutionize electronics manufacturing paradigms*, IEEE, (2017).
- [6] W. H. J. Q. L. Z. CHENG ZHONG, YIDA DENG AND J. ZHANGD, *A review of electrolyte materials and compositions for electrochemical supercapacitors*, The Royal Society of Chemistry, (2015).
- [7] D. C. COMPANY, *Triethylene glycol*, February 2007.
- [8] D. M. U. DR. MADAN DUBEY, DR. RAJU NAMBARU, *Graphene-based nanoelectronics (fy11)*, Journal of Engineered Fibers and Fabrics, (January 2012).
- [9] J.-H. Y. S. H. C. C. R. M. C. P. G. JUNG BIN IN, BEN HSIA, *Facile fabrication of flexible all solid-state micro-supercapacitor by direct laser writing of porous carbon in polyimide*, Elsevier, (2014).

BIBLIOGRAPHY

- [10] Z. P.-Y. L. C. G. Y. J. R. Y. N. D. K. Q. Z.-Y. Y. H. F. G. R. LEI LI, JIBO ZHANG AND J. M. TOUR, *High-performance pseudocapacitive microsupercapacitors from laser-induced graphene*, WILEY-VCH Verlag GmbH Co. KGaA,, (2015).
- [11] Z. N. LILI LIU AND J. CHEN, *Design and integration of flexible planar microsupercapacitors*, Nano research, (2016).
- [12] Y. L. Z.-Y. J. Y. P. Y.-Q. C. D.-Y. W. X.-G. T. J.-C. Y. N.-Q. D. Y. Y. . T.-L. R. LU-QI TAO1, HE TIAN, *An intelligent artificial throat with sound-sensing ability based on laser induced graphene*, Nature communications, (February 2017).
- [13] S. Y. NANSHU LU, CHI LU AND J. ROGERS, *Highly sensitive skin-mountable strain gauges based entirely on elastomers*, Advanced functional materials, (2012).
- [14] K. W. O'BRIEN, *Synthesis of functionalized poly(dimethylsiloxane)s and the preparation of magnetite nanoparticle complexes and dispersions*, (2003).
- [15] M. S. R. RAMYA, R. SIVASUBRAMANIAN, *Conducting polymers-based electrochemical supercapacitors—progress and prospects*, ELSEVIER, (2012).
- [16] W. Y. RAHIM RAHIMI, MANUEL OCHOA AND B. ZIAIE, *Highly stretchable and sensitive unidirectional strain sensor via laser carbonization*, ACS Publications, (2015).
- [17] G. C. STEFANO STASSI, VALENTINA CAUDA AND C. F. PIRRI, *Flexible tactile sensing based on piezoresistive composites: A review*, Sensors, (2014).
- [18] M. M. STEPHANIE FLORES ZOPF, *Screen-printed military textiles for wearable energy storage*, Journal of Engineered Fibers and Fabrics, (2016).
- [19] WIKIPEDIA CONTRIBUTORS, *Polydimethylsiloxane — Wikipedia, the free encyclopedia*, 2018.
[Online; accessed 30-November-2018].
- [20] —, *Ragone plot — Wikipedia, the free encyclopedia*, 2018.
[Online; accessed 21-November-2018].
- [21] —, *Strain gauge — Wikipedia, the free encyclopedia*, 2018.
[Online; accessed 17-November-2018].

- [22] L. S. P. S. C. J. A. YIEU CHYAN RUQUAN, YE YILUN AND J. M. TOUR, *Laser-induced graphene by multiple lasing: Toward electronics on cloth, paper, and food*, (2017).
- [23] S. ZHANG AND N. PAN, *Supercapacitors performance evaluation*, WILEY-VCH Verlag GmbH & Co. KGaA, Weinheim, (2014).
- [24] Z. G.-Y. ZHAO JING AND S. DONG-XIA, *Review of graphene-based strain sensors*, Chinese Physical Society and IOP Publishing, (2013).
- [25] J. A. M. D. Z. Y. L. P. R. S. J. L. ZHIWEI PENG, RUQUAN YE AND J. M. TOUR, *Flexible boron-doped laser-induced graphene microsupercapacitors*, ACSNANO, (2015).

